Toward a hydroclimatic reconstruction for the Río Santa Cruz, Patagonia, Argentina

Master's Thesis

Faculty of Science

University of Bern

presented by

Erin Gleeson

2009

Supervisor:

Dr. Jan Esper
Swiss Federal Research Institute for Forest, Snow and Landscape Research,
and Oeschger Centre for Climate Change Research

Co-Supervisor:

Dr. Ricardo Villalba
Laboratorio de Dendrocronología e Historia Ambiental, IANIGLA, CONICET

Advisor:

Dr. David Frank
Swiss Federal Research Institute for Forest, Snow and Landscape Research,
and Oeschger Centre for Climate Change Research

Declaration

under Art. 28 Para. 2 RSL 05

Last, first name: Gleeson, Erin

Matriculation number: 07-108-129

Programme: Climate Sciences

Bachelor ☐ Master ■ Dissertation ☐

Thesis title: Toward a hydroclimatic reconstruction for the Río Santa Cruz, Patagonia, Argentina

Thesis supervisor: Dr. Jan Esper

Dr. Ricardo Villalba

I hereby declare that this submission is my own work and that, to the best of my knowledge and belief, it contains no material previously published or written by another person, except where due acknowledgement has been made in the text. In accordance with academic rules and ethical conduct, I have fully cited and referenced all material and results that are not original to this work. I am well aware of the fact that, on the basis of Article 36 Paragraph 1 Letter o of the University Law of 5 September 1996, the Senate is entitled to deny the title awarded on the basis of this work if proven otherwise.

.....

Place, date

.....

Signature

Summary

Snaking seaward from the eastern slope of the Andes, the Río Santa Cruz occupies southern Argentina's largest basin and is vital to the region's economic and ecologic health, including tourism, irrigation, habitat conservation and hydroelectric power. River discharge is derived primarily from snow and glacial melt, which is in turn governed by the complex interaction between climatic conditions and the dynamics of the South Patagonian Ice Field. However, this interaction is poorly understood and instrumental climate and streamflow records for the region are limited in both spatial and temporal coverage. In the face of a changing climate and widespread glacial recession, a more thorough understanding of the region's hydroclimatic variability is essential to the sound management of its water supplies.

Tree-rings provide one means of estimating climate variability in southeastern Patagonia over the last several centuries by providing long, well-replicated records with annual resolution. To this end, 200-year long *Nothofagus pumilio* tree-ring chronologies from six sites in the headwaters of the Río Santa Cruz were developed. Strongly correlated chronologies were combined to create four regional composite chronologies. These chronologies were then compared with instrumental climate and streamflow records from the region to identify the key factors influencing tree growth. Similarly, instrumental climate and streamflow records were compared with each other and with the dominant atmospheric circulation patterns to determine how streamflow in southeastern Patagonia is influenced by climate and the dynamics of the South Patagonian Icefield.

Analysis of the tree-ring chronologies indicate that trees in southeastern Patagonia respond to a common climatic signal. In particularly, the composite chronologies show a strongly seasonal response to both temperature and discharge, which suggests that tree growth is influenced by a mixed temperature-soil moisture signal. This signal is further complicated by a strong oscillatory relationship with the Mean ENSO Index and a generally positive correlation with the AAO during the spring (September-December).

This study explores the challenges of developing a hydroclimatic reconstruction in a region characterized by mixed climatic signals, complex topography and limited instrumental records. The dominant climatic, hydrological and geographic factors influencing tree growth are described and future steps toward building a multi-century reconstruction of hydroclimatic variability in the Santa Cruz basin are considered.

Contents

Chapter 1 - Introduction

1.1 Overview

Concerns about future water supplies have dominated scientific, economic and political conversations in recent years as rapid population growth and a changing climate prompt questions about resource availability. In the coming decades, diminished water quality and reduced availability are expected to be the primary limiting factors on economic growth and the greatest threats to environmental health in many regions of the world (Bates et al., 2008). Increasing and diverse demands on this finite resource will have repercussions on all aspects of society, from agriculture and industry to energy and environmental sustainability. Nearly half the world's population will inhabit areas subject to severe water stress by 2030 (OECD, 2008), a situation that will strain the ingenuity of resource planners worldwide as a changing climate reduces the predictability of water resources.

Barnett et al. (2005) have suggested that changes in the hydrological cycle may be even more serious in regions that depend heavily on glacial meltwater for their main dry-season water supply. The focus of this research, the Santa Cruz basin in Patagonia, Argentina, is one such region. Here, glaciers of the South Patagonian Icefield act as giant freshwater reservoirs, storing large quantities of water for thousands of years. During the dry summer months, the release of some of this stored water sustains downstream communities. As long as the rate of accumulation exceeds the rate of discharge, downstream users are guaranteed a relatively constant supply of freshwater. Barnett et al. (2005) identified the southern Andes as a region where there is not adequate reservoir storage capacity to buffer shifts in the seasonal hydrograph. If glaciers in the Andes continue to retreat at their current rate, communities that now depend on the water stored in glaciers will be left to depend on the vagaries of seasonal snowpack.

The majority of water consumed by downstream users in the Santa Cruz basin is extracted directly from the Río Santa Cruz, which runs east from the foothills of the Andes to the Atlantic Ocean. River discharge is sensitive to long-term changes in both precipitation and temperature, especially in meltwater-dominated regions of the world. Changes in the amount of precipitation -- particularly snow accumulation -- are reflected in changes in the runoff volume. In turn, changes in temperature affect the timing of runoff from meltwater as well as evapotranspiration. As both the natural environment and human infrastructure and practices have adapted to function on a certain hydrological calendar and with a given average annual supply of water, a shift in the mean, variance or seasonality of the local hydrological cycle can result in severe repercussions to both the natural and human environment. The diagram in Figure 1.1 illustrates how a change in dry season runoff may lead to socio-economic conflict as population growth places increasing demand on water resources.

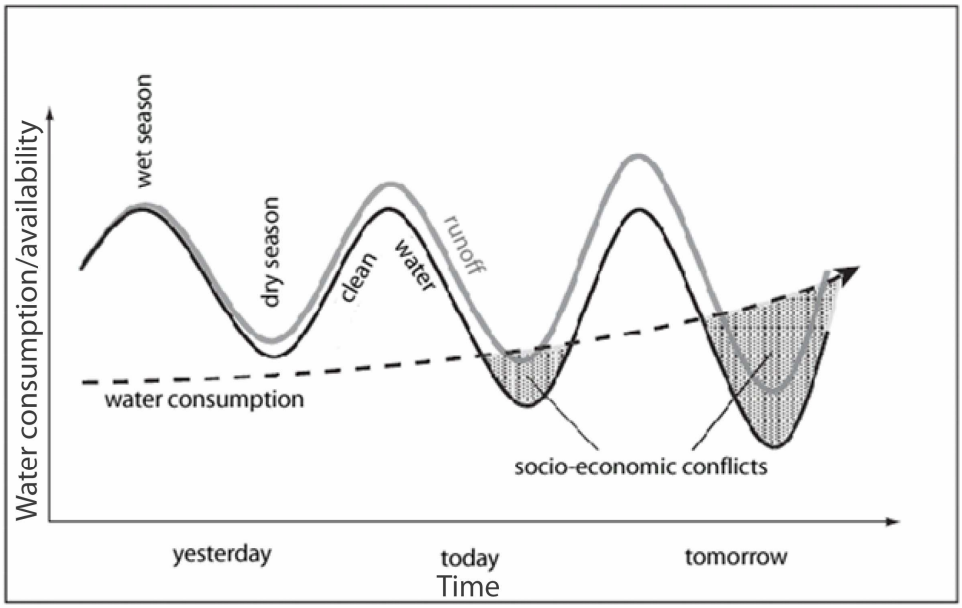

Figure 1.1. The widespread retreat of glaciers, in addition to increasing demands on water resources by a growing population, may lead to socio-economic conflict in the future. As the glacial reservoir shrinks, runoff variability increases and less and less water is available during the dry season, when it is needed most by agriculture, tourism, and other competing sectors. Adapted from Kaser et al., 2001.

If future water problems are to be properly anticipated, it is necessary to improve our understanding of the issues involved on a regional basis. This is particularly true of areas that have limited climatic and hydrological records, such as Patagonia Argentina. Although Patagonia is unlikely to see the dramatic population growth already taking place in the drought-prone north, it plays an important role in the country's hydropower and tourism industries. The main rivers in semi-arid Patagonia, including the Río Santa Cruz, produce more than 25% of the total energy consumed in Argentina (Quintela et al., 1996). In the next five years, two large dams will be constructed along the Río Santa Cruz, creating 5,000 new jobs and supplying 16% of Argentina's hydropower (Quiroga, 2008). In a region where river discharge is governed by complex interactions between climatic conditions and the dynamics of the South Patagonian Ice Field and where very few long, homogeneous and complete station records exist, resource planning is difficult.

Fortunately, dendrohydrology offers accurate methods for studying long-term hydrologic variability at regional scales. Annual tree rings can augment gauged hydrologic data by extending hydrologic records for hundreds or even thousands of years (Cleaveland, 2000). In many temperate and boreal regions, trees are faithful recorders of environmental variability, including changes in temperature and precipitation. The relationship between tree growth and water availability allows us to extend our knowledge of hydrologic variability in regions where instrumental data is lacking. This study explores the potential use of *Nothofagus pumilio* for extending our temporal understanding of hydroclimatic variability in southeastern Patagonia.

1.2 The physical geography of southern Patagonia

Patagonia is a broad geographical term describing the southernmost portion of South America from about 36°S to the tip of Tierra del Fuego. The high spine of the Andes divides Patagonia between Chile to the west and Argentina to the east and cradles the Patagonian icefields between its peaks south of 46°S. Straddling both flanks of the Andes, Patagonia is a land of contrasting extremes. If one were to walk a latitudinal transect across Patagonia at 50°S from the Chilean coast on the Pacific Ocean to the Argentinean coast on the Atlantic Ocean, one would first encounter dense temperate rainforests cloaking the western flank of the Andes. Above the tree line, the ice-clad peaks of the cordillera loom over the inhospitable expanse of the South Patagonian Icefield, the primary source of water in southeastern Patagonia. Some 150 km inland, the Andes disappear into the featureless plains of the Argentine Patagonian steppe, where the dry, persistent winds of the westerlies create a harsh, arid land. At the foot of the Andes lie some of the largest lakes in the Southern Hemisphere, into which the enormous tongues of the South Patagonian Icefield calve. The complex interaction between climate and topography makes southern Patagonia a fascinating place to study past climates.

1.2.1 Climate

The north-south trending Andean range creates a strong topographic barrier that has a profound influence on the climate and hydrology of southern Patagonia. Moisture-laden westerlies deposit the majority of their precipitation on the western slope of the Andes and over the South Patagonian Icefield, then descend over the eastern slope cold and parched. At 50°S, drainage of the South Patagonian Icefield to the east supplies the majority of the region's water needs.

Together, southern Patagonia and Tierra del Fuego form the only extensive landmass between 46° and 56° in the Southern Hemisphere. The climate is largely determined by the prevailing westerly winds from the Pacific, which occur between the semi-permanent subtropical high and the subpolar low. The westerlies reach their greatest intensity over southern Patagonia, at about 50°S (Garreaud et al., 2009). Here, the north-south trending spine of the Andes decreases in height to an average of 2200 m a.s.l., allowing an intrusion of Pacific moisture over the eastern slope (Pasquini et al., 2008). The westerly winds blow throughout the year and are strongest and most persistent in (austral) summer. However, the moisture-laden air is intercepted by the western slope of the Andes, leaving the westerlies to blow cold and moisture-depleted over the eastern slope. As a result, annual rainfall on the Chilean side of the Andes is as much as 8,000 mm (Rosenblüth et al., 1995), whereas in eastern Patagonia precipitation decreases to less than 250 mm. According to Jobbágy et al. (1995), the distance from the Andes explains 94% of the spatial variability in the mean annual precipitation.

It should be noted that seasons in the Southern Hemisphere are reversed in comparison to those in the Northern Hemisphere. Thus, January corresponds to high summer in Patagonia whereas July coincides with midwinter.

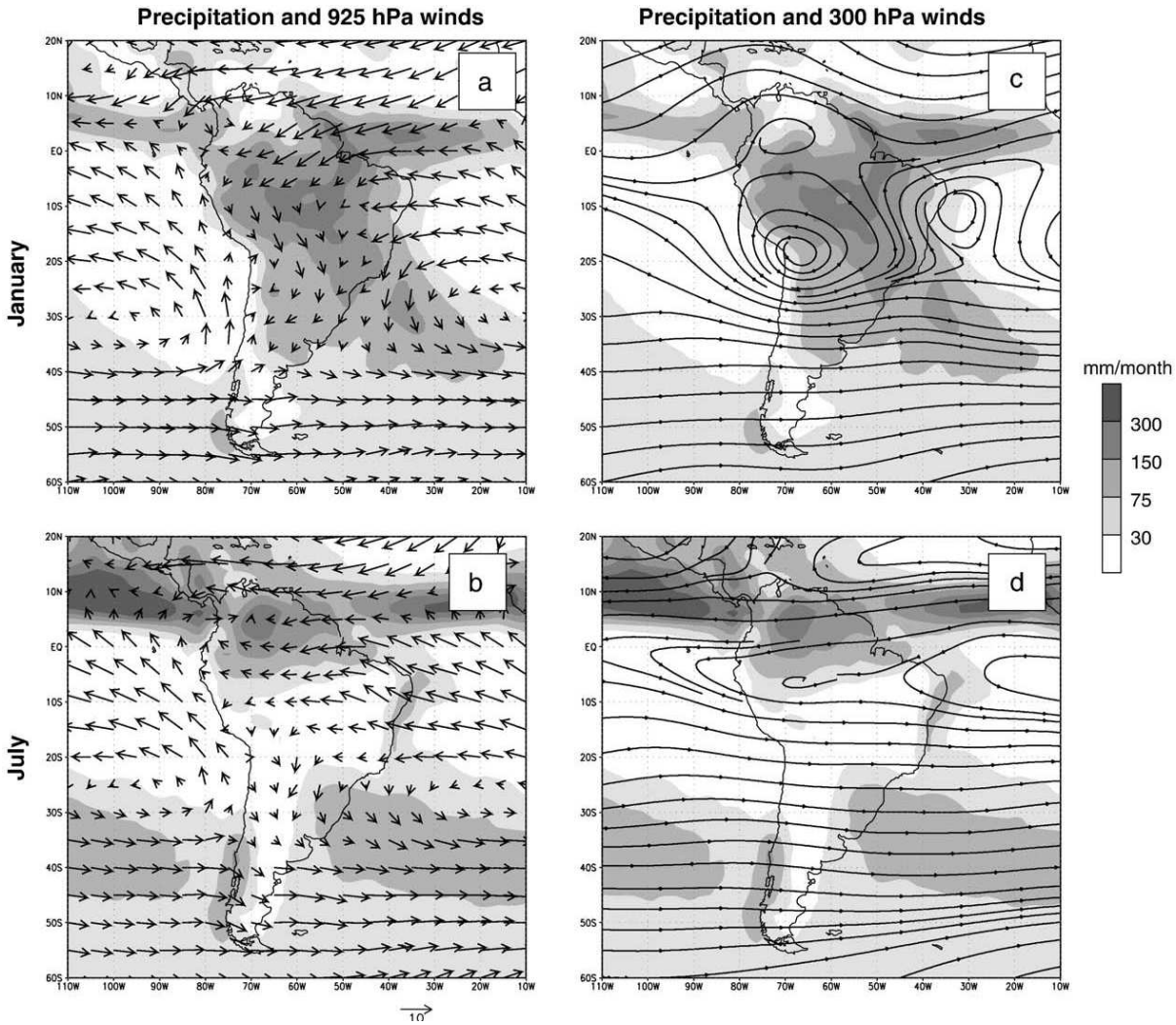

Figure 1.2. Left panels: long-term mean CMAP precipitation (shaded — scale at right) and 925 hPa wind vectors (arrows — scale at bottom) for (a) January and (b) July. Right panels: long-term mean precipitation (shaded — scale at right) and streamlines at 300 hPa (streamlines) for (c) January and (d) July. South of 40°S, the flow of the westerlies predominate throughout the year over the ocean and the continent. The precipitation shows a marked west-east asymmetry. Over the southern extreme of the continent, the westerlies are stronger during the summer and reach their maximum values between 45 and 55°S. The jet stream expands northward to Ecuador during the winter but is much weaker, especially at 55°S. From Garreaud et al. 2009.

The majority of precipitation occurring at the latitude of the study area falls in autumn and winter. At El Calafate, the meteorological station closest to the study area, peak precipitation occurs in May (average 29.6 mm) and the total annual mean is 203 mm. Almost two-thirds of all precipitation at El Calafate occurs during the fall and winter months (April-September). Mean annual air temperature is 7.5°C, with an average monthly maximum of 13°C in January and a minimum of 0.7°C in July. The annual range of monthly temperature is lower in Patagonia than at similar latitudes in the Northern Hemisphere primarily because of the lack of significant land mass in the Southern Hemisphere. A 53-year meteorological record (1937-1990) at El Calafate (Ibarzabal et al., 1996) shows a slight rising trend in temperature and a decreasing trend in precipitation. Rosenblüth et al. (1995) have observed a surface warming of up to 0.03°C/year from 46° to 55°S over the past century, as well as a notable decrease in precipitation on the western side of the Andes at 53°S.

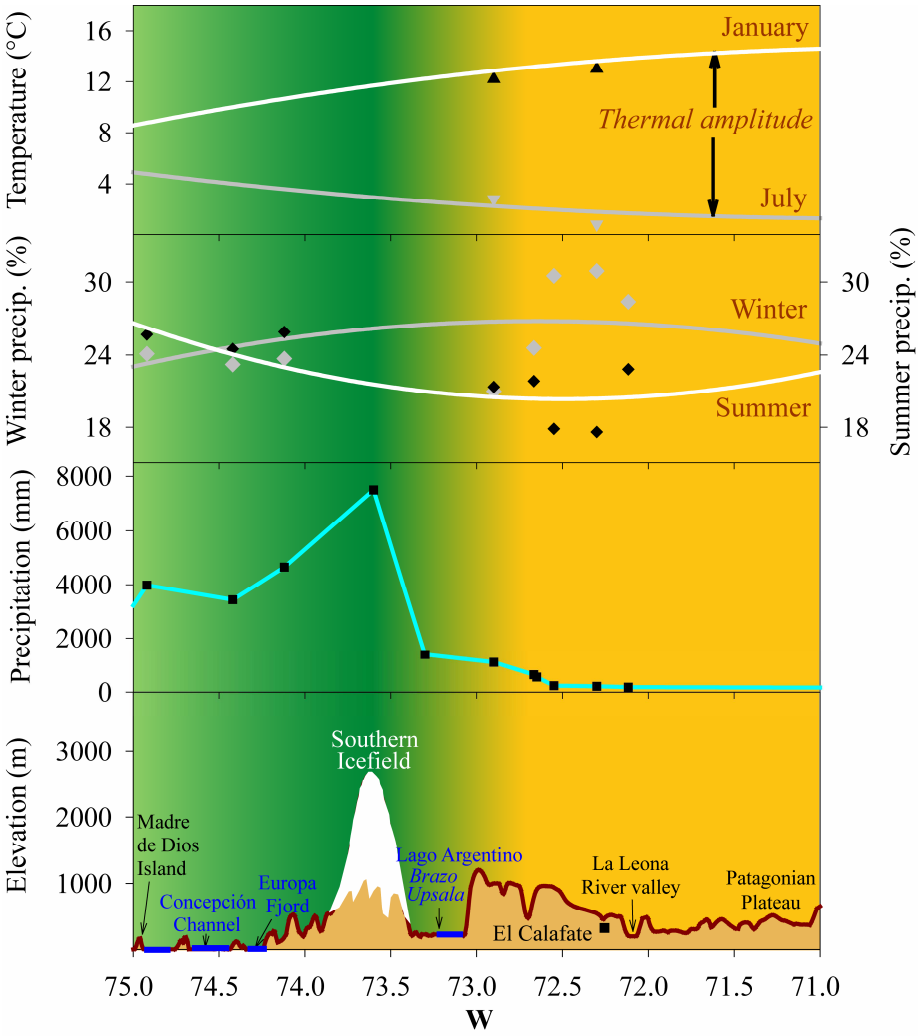

Figure 1.3. Transect across the southern Andes at approximately 51°S showing changes in mean January and July temperatures a) in seasonal (summer and winter) precipitation distribution b) and in total annual precipitation c) associated with topography and d) distance from the Pacific Ocean. Locations of the meteorological stations are indicated by triangles in a), diamonds in b) and squares in c). Meteorological data are from stations located in the latitudinal band between 49°S and 53°S. From Villalba et al., 2003.

1.2.2 The South Patagonian Icefield

The South Patagonian Icefield (SPI) is the largest temperate ice body in the Southern Hemisphere and third in size globally after the Greenland and Antarctic ice sheets. Locally known as the Hielo Patagónico Sur, the SPI extends north-south for 350 km between 48°20'S and 51°30'S. Stretching over approximately 13,000 km^2, the SPI is cradled in the southern Andes between approximately 73°05' and 73°45'W. The icefield nourishes numerous large outlet glaciers, most of which terminate at calving cliffs in the Chilean fjords or in the big Argentine lakes (Warren and Sudgen, 1993). Two of the largest glaciers in Southern America – Upsala and Viedma – drain into lakes Argentino and Viedma, which in turn feed the Río Santa Cruz. Frequent calving commonly produces icebergs with volumes of several million cubic meters (Warren and Sudgen, 1993).

As a result of the interaction between the flow of the westerlies and the topography of the Andes, the western margin of the SPI receives considerable precipitation, with an estimated annual average of 10-m water equivalent on the icefield plateau (DGA, 1987). In contrast,

the eastern margin of the SPI receives little precipitation, amounting to a few hundred millimeters per year in the Argentine Patagonian plateau. The mean annual temperature of the marginal areas of the SPI is approximately 6°C, which allows for the existence of a unique ecosystem of southern beech (*Nothofagus*) forests at the glacier fronts (Peña and Gutiérrez, 1992). A growing number of dendrochronological studies take advantage of these *Nothofagus* forests to reconstruct glacier dynamics, precipitation and temperature (e.g., Villalba et al., 1990; Villalba et al., 1998; Lara et al., 2001; Aravena et al., 2002).

Despite its size and notwithstanding significant advances in research over the last decade, the SPI remains among the least known of the world's icefields. The first complete inventory for the SPI was compiled in 1996 by Aniya and others, in which 48 major outlet glaciers and over 100 small cirque and valley glaciers were identified. In a later review Aniya (1997) showed that all but two of the 48 glaciers retreated or remained stagnant over the 1945-1986 period, resulting in a net ice area loss of about 200 km^2. Comparing satellite-derived topography with earlier cartography, Rignot et al. (2003) found thinning rates between 1995 and 2000 that were more than double the rates between 1970 and 1995. They determined that a substantial part of the thinning is due to excess longitudinal thinning and accelerated calving, as well as to climate warming.

Based on NCEP-NCAR Reanalysis data used to investigate changes in precipitation and snowfall over the Patagonia icefields during 1960-1999, Rasmussen et al. (2007) provide further support for this theory. Although total precipitation over the icefields has not changed, warming has caused a decrease in the proportion falling as snow. Precipitation that falls as rain has a higher kinetic energy than snow and enhances meltwater production, which in turn increases basal lubrication and allows faster flow rates. Without a corresponding increase in snow accumulation, the glaciers thin as they flow away from the icefield.

As the glaciers of the SPI retreat, thin and calve, the water they have stored as ice for hundreds of years is released. Using remote sensing data, Aniya calculated a sea level rise contribution of 0.038 ± 0.015 mm/yr over the period from 1945-1996 (1999). Chen et al. (2007) used changes in Earth's gravity field observed from space by the Gravity Recovery and Climate Experiment (GRACE) to compute a contribution to sea level rise of 0.078 ± 0.031 mm/yr. Comparing digital elevation models generated from the 2000 Shuttle Radar Topography Misson with earlier cartography, Rignot et al. (2003) estimated that between about 1970 and 1995, ice loss on the SPI was 13.5 ± 0.8 km^3/year. Combined with the contribution of the North Patagonian Icefield, the total volume loss over the 1970-1995 period is equivalent to a sea level rise of 0.042 ± 0.002 mm/year. Ice loss and contribution to sea level rise over the 1995-2000 period was found to be over double that of the previous three decades. As the authors point out, the Patagonian glaciers cover an area five times *smaller* than their Alaskan counterparts, yet the contribution of Patagonian glaciers to sea level rise is 1.5 times *larger* than that of Alaskan glaciers. This alone suggests the need for a better understanding of Patagonian climate and hydrology.

1.2.3 Hydrology of southeastern Patagonia

At about 50°S, the South Patagonian Icefield drains into lakes Argentino and Viedma, which in turn feed the Río Santa Cruz. The waters of Lago Viedma are transported to Lago Argentino via the river La Leona, which supplies about 35% of the total Río Santa Cruz annual discharge (Depetris and Pasquini, 2000). At its eastern end, Lago Argentino gives

birth to the Río Santa Cruz, which then winds some 383 km across the Santa Cruz province before emptying into the Atlantic. The Santa Cruz basin covers 29,685 km^2. Like most rivers in Patagonia, the Río Santa Cruz is exposed to the influence of Pacific climate because the Andean Cordillera loses height south of ~47°S, allowing the intrusion of Pacific moisture (Pasquini et al., 2008). Indeed, all rivers in southern Patagonia are controlled by precipitation from the Pacific: Precipitation from the Atlantic plays only a very minor role along the coastal region. As a result, mean annual precipitation is unevenly distributed over the basin, with the vast majority falling as snow over the South Patagonian Icefield. Not surprisingly, discharge on the Santa Cruz is driven primarily by snowmelt and ice ablation and peaks in late summer (March). The mean discharge at the Charles Fuhr hydrological station on the Río Santa Cruz in March is 1,278 m^3/s compared to 278 m^3/s in September, typically the month with the least discharge (Valladares, 2004). Figure 1.4 illustrates the differences in discharge volume, river size and streamflow variability of the five gauged rivers in the Santa Cruz Basin.

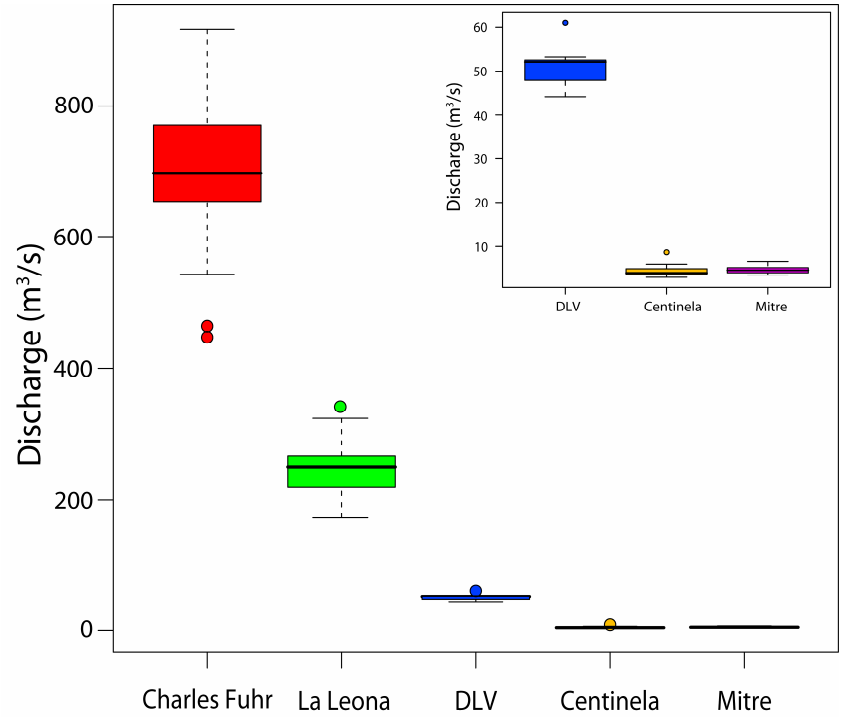

Figure 1.4. Streamflow varies widely among the five rivers in the Santa Cruz Basin. Discharge at the Charles Fuhr station is several orders of magnitude greater than that in the smaller streams and nearly three times that of the next largest river, La Leona. The inset shows discharge for the three smaller rivers in greater detail.

It should be noted that the Perito Moreno Glacier (50°30'S, 73°00'W) periodically dams one of Lake Argentino's lateral channels. The Perito Moreno has triggered periodic outburst floods in the Río Santa Cruz whenever the ice dam collapses in response to the rising water level of the dammed branch (Depetris and Pasquini, 2000). They identified discharge anomalies in the Santa Cruz related to snout collapses in 1956, 1966, 1970, 1972, 1975, 1977, 1980, 1984, and 1988. Collapses occurring prior to the period of record are known for 1917, 1934, 1935, 1940, 1942, 1947, 1952, and 1953. The authors note that most glacier ruptures appear to be linked to the El Niño-Southern Oscillation (ENSO) and roughly coincide with or follow El Niño events. However, these anomalies are sufficiently small not to be considered in this study.

1.3 Southern Patagonia and dendrochronology

The geographic complexity of southern South America makes it an interesting region for understanding significant environmental variations occurring in the past several hundred years. In this sparsely populated region, proxies such as tree rings may provide the best source of information. In southwestern Patagonia, the subantarctic forests are dominated by *Nothofagus* species from sea level to treeline in the Andes (Roig and Villalba, 2008) and provide a rich source of climatic information. The following section describes the study species, *Nothofagus pumilio*, in detail. Dendrohydrology and the potential of *N. pumilio* in dendrohydrologic studies are also discussed.

1.3.1 *Nothofagus pumilio*

Nothofagus pumilio (Poepp. et Endl.) Krasser, locally known as lenga, is a deciduous tree species that dominates the upper tree line of the Chilean and Argentinean Andes between 35º36' and 55ºS (Donoso, 1993). In Argentina, pure stands of *N. pumilio* cover about 1 million ha between its northernmost extent in Neuquén and Tierra del Fuego (2200 km). The vast geographic distribution of *N. pumilio* implies a broad tolerance range, as it is distributed along a north-south temperature gradient and a strong west-east precipitation gradient (Donoso, 1993). Indeed, low temperatures most of the year, heavy snowfall, rainfall distribution with a strong winter maximum and dry summers, a short vegetative period and frosts occurring throughout the year are common features of this species' environment (Cwielong and Rajchenberg, 1995).

N. pumilio forests occur from sea level to tree line, which occurs between about 1000 and 1100 meters above sea level in the study area. At lower elevations, *N. pumilio* grows to a height of ~20-25 m. Tree height decreases with altitude and at tree line *N. pumilio* may occur as 1-4 m tall krummholz. Near the center of its distribution (~41 ºS) mean annual precipitation exceeds 5,000 mm on the western side of the Andes and is less than 800 mm at its easternmost extent (Veblen et al., 1996). Annual precipitation declines to about 400 mm at the species' southernmost extent, and much of that precipitation falls as snow at altitudes above 700-800 m in the region of El Chalten. The moist forests of the western slope are dominated by the evergreen *Nothofagus betuloides*; following the decreasing precipitation gradient eastward, deciduous forests of *N. pumilio* dominate the landscape (Aravena et al., 2002). Figure 1.5 shows the geographic distribution of *N. pumilio* as well as the anatomical characteristics of the rings.

Throughout its range, *N. pumilio* is typically the primary tree species colonizing well-drained slopes, where it forms dense and generally pure uneven-aged stands (Roig and Villalba, 2008). However, it may also occur in mixed stands with a variety of other *Nothofagus* species, as is the case in several of the sites used in this study. In several instances, *N. betuloides* was encountered in the study areas. The evergreen *N. betuloides* becomes dominant on the western side of the Andes south of 48°S, where cold, humid conditions prevail (e.g., Roig and Villalba, 2008). *N. betuloides* has been successfully employed in climate reconstructions (e.g., Boninsegna et al., 1989; D'Arrigo and Villalba, 2000), but the presence of numerous, extremely narrow rings make dating very difficult. The species is not used in the present study.

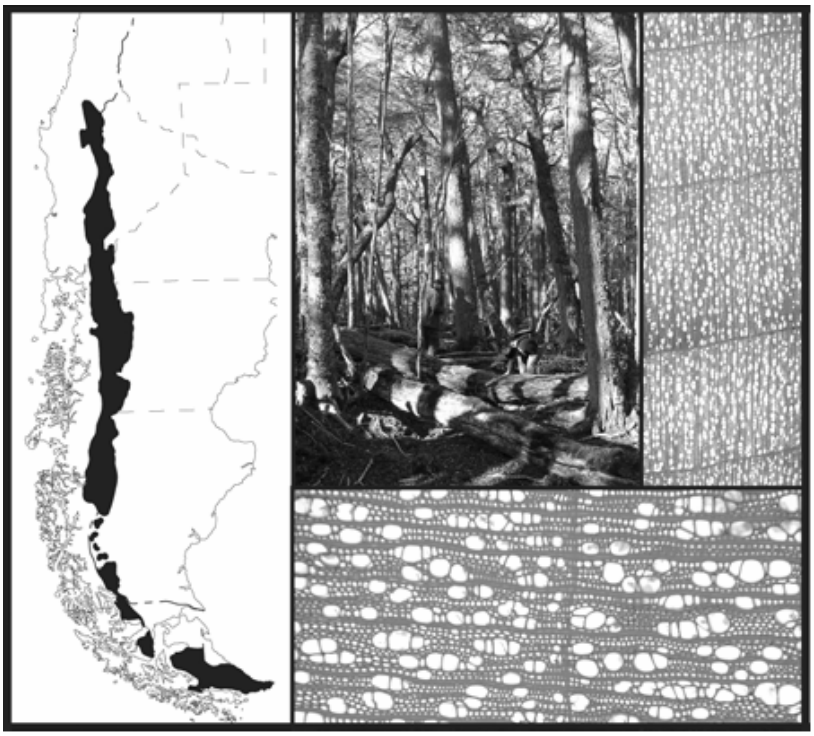

Figure 1.5. Geographic distribution of *Nothofagus pumilio* and tree-ring anatomical characteristics. From Roig and Villalba, 2008.

Reliable chronologies of up to 400 years can be obtained from *Nothofagus* species, which live to a maximum age of approximately 500 years (Roig and Villalba 2008). This is primarily due to a widespread occurrence of fungal infection in *N. pumilio.* Wood rot is the most important and costly problem affecting the economic utilization of lenga and heart-rots are the main type of rot in living lenga (Cwielong and Rajchenberg, 1995). The majority of the trees sampled for this study are assumed to be affected by *Postia pelliculosa*, a species of fungi that first causes the wood to darken and then deteriorate: the wood assumes a cubical and punky consistency that, once advanced, makes ring measurement impossible.

1.3.2 Dendrohydrology and *Nothofagus pumilio*

N. pumilio has diffuse-porous rings with obscure boundaries, particularly in the lighter sapwood. Masiokas and Villalba (2004) reported the presence of intra-annual bands in the wood of *N. pumilio* in southern Patagonia and noted that the formation of intra-annual bands appears to be in response to anomalously warm and dry springs followed by wet and warm late summers. It has been noted that the growth of *N. pumilio* is particularly affected by temperature restrictions throughout its more than 2000 km latitudinal distribution (Lara et al., 2005). As such, a large number of chronologies have been developed on both sides of the Andes with the goal of better understanding long-term temperature changes on either side of the cordillera (e.g., Boninsegna et al., 1989; Aravena et al., 2002; Villalba et al., 2003; Villalba et al., 1997b). More recently, the utility of the species for precipitation reconstructions has been demonstrated by Masiokas and Villalba (2004). However, to date no streamflow reconstructions have been developed for South America using *Nothofagus pumilio*.

Stockton and Jacoby's landmark reconstruction (1976) of Colorado River flow was the first tree-ring based effort aimed at the quantitative reconstruction of streamflow records. The Stockton and Jacoby study famously showed that the Colorado River Compact -- an agreement signed in 1922 by seven U.S. states regarding the allocation of Colorado River water -- was based on the wettest multidecadal period in the previous 400 years. In 1944 the compact was further amended to include Mexico. Today the Compact is regarded as a milestone achievement in water law (McClurg, 2007) but the overoptimistic allocations, based on a very short streamflow record, continue to challenge resource managers. Demands on water resources by mushrooming populations and agriculture, hydroelectricity and natural habitats have been further compounded by persistent drought. More realistic, long-term estimates of mean annual streamflow, such as those derived from tree rings, may help resource managers better plan for the future.

Unfortunately, in many parts of the world instrumental data and particularly streamflow records are limited to the last several decades at best. In the Santa Cruz basin, only two streamflow records dating back to the 1950s are available, and these are incomplete. Nevertheless, sound water resource planning depends on long-term, high-quality records of streamflow and precipitation. Table 1.1 provides a summary of streamflow reconstructions to date. Tree rings have been successfully employed to reconstruct precipitation, streamflow and other meteorological variables for various regions worldwide (e.g., Fritts, 1971; Lough and Fritts, 1985; Briffa et al., 1990; D'Arrigo and Jacoby, 1991; Stahle and Cleaveland, 1993; Cook et al., 1999; Cleaveland, 2000; Esper et al., 2007).

Previous work in Argentina and Chile has demonstrated that *N. pumilio* provides climate sensitive tree-ring records for approximately the last 400 years. Reconstructions of temperature, summer transpolar and summer mean sea level pressures (Villalba et al., 1997b; D'Arrigo and Villalba, 2000) have been successfully developed for the south Patagonian Andes. *N. pumilio* has also been used to reconstruct spring snow cover duration (Villalba et al., 1997a) and summer precipitation (Lara et al., 2001) in northern Patagonia. Although *N. pumilio* is often used in conjunction with other tree species such as *Austrocedrus chilensis* and *Araucaria araucana* for climate reconstructions in the north, it is the prime target for reconstructions in the south because of its widespread occurrence.

Only three streamflow reconstructions have been developed in southern South America. A recent study by Lara et al. (2008) presented a reconstruction for the Puelo River in Chile at 41°S latitude back to 1599 using *Austrocedrus chilensis* and *Pilgerodendron uviferum*. The study by Lara et al. is the first streamflow reconstruction developed in western South America. In Argentina, two prior streamflow reconstructions exist. In northern Patagonia, *Araucaria araucana* and *Austrocedrus chilensis* tree rings have been used to extend the flow series for the Limay and Neuquén rivers (39°S) back to 1601 (Holmes et al., 1979). In Mendoza Province, tree rings from *A. chilensis* have been used to reconstruct Atuel River streamflow back to 1576 (Cobos and Boninsegna, 1983).

The only streamflow reconstruction employing *Nothofagus*, however, is the 1987 study by Norton, who successfully reconstructed streamflow for the Hurunui River in New Zealand back to 1879. Norton employed *Nothofagus solandri*, a species of southern beech endemic to New Zealand, in his reconstruction. Like *N. pumilio*, *N. solandri* is a hardy, widespread tree that often forms the tree line and lives to a maximum age of about 300 years (Norton, 1983). Norton demonstrated a strong dependence of growth on summer precipitation and, using this

relationship, developed regressions between regional precipitation and Hurunui River flow that explain 46% and 52% of the variance over the calibration period, respectively.

Table 1.1. Summary of tree-ring based streamflow reconstructions worldwide. This summary indicates the range of streamflow reconstructions that have been developed over the last 40 years.

Region	River/region	Period	Tree species[a]	Source
Eastern North America	Potomac River, MD	1730-1977	TSCA, QUAL, QUPR, PIRI	Cook & Jacoby, 1983
	White River, AR	1023-1985	TADI	Cleaveland, M.K., 2001
Western North America	Colorado River, AZ/CO	1564-1961	unknown	Stockton & Jacoby, 1976
	Salt & Verde Rivers, AZ	1580-1979	PIPO, PIED	Smith & Stockton, 1981
	Sacramento, Feather, Yuba and American Rivers, CA	1560-1980	PIPO, PIJE, JUOC, PILA	Earle et al., 1993
	Upper Gila River, AZ	1663-1985	PIPO, PIED, PISF, ABCO, PSME	Meko & Graybill, 1995
	Sacramento River, CA	869-1999	SEGI, QULO, TSME, PICO, PILO, PIBA PIMO, JUOC, PILA, PIPO, PIJE, QUDO	Meko et al., 2001
	Yellowstone River	1706-1977	PSME	Graumlich et al., 2003
	Columbia River, WA	1750-1987	ABLA, JUOC, LALY, PCEN, PIFL, PIPO, PSME	Gedalof et al., 2004
	Ashley Creek , UT	1637-1970	PSME, PIED	Carson & Munroe, 2005
	Sacramento (CA) and Blue (CO) Rivers	1440-1977	PSME, PSMA, PIPO, PIJE, PIED	Meko and Woodhouse, 2005
	Colorado River, AZ	1490-1997	PIPO, PIED, PIFL, PSME	Woodhouse et al., 2006
	Jordan River, UT	1178-2006	PIFL, PSME	Tikalsky et al., 2007
	Yampa, Whiterocks, Uncompahgre Rivers, CO/UT/WY	1500-1980	PIFL, PIED, PIPO, PSME	Timilsena et al., 2008
	Wind River, WY	1672-2000	PIED, PIFL, PSME	Watson et al., 2009
Canada and Mexic	North Saskatechewan River	883-1996	PIFL, PCMA	Case et al., 2003
	South Sastkatchewan River	1470-1992	PIFL, PCMA	
	Sasktachewan River	1671-1996	PIFL, PCMA	
	Gulf of California watershed, MX	1712-1993	PSME, PILA	Brito-Castillo et al., 2003
	Oldman River, Saskatchewan	1618-2004	PIFL, PSME	Axelson et al., 2009
	Bow River, Saskatchewan	1400-2008	PIFL, PSME	
Europe	Wensum River, Britain	1838-1980	QUPE, QURO	Jones et al., 1984
	Exe River, Britain	1856-1980	QUPE, QURO	
	Wye River, Britain	1860-1980	QUPE, QURO	
	Filyos River, Turkey	1650-1998	PINI, PISY, ABBN +others	Akkemik et al., 2007
Asia, India, Oceania	Hurunui River, New Zealand	1879-1977	NOSO	Norton, D.A., 1987
	Kherlen River, Mongolia	1651-1995	PISY, LASI	Pederson et al., 2001
	Yellow River, China	1409-2001	JUPR	Gou et al., 2007
	Manasi River, China	1629-2000	PCSH	Yuan et al., 2007
South America	Neuquén & Limay Rivers, Argentina	1601-1968	AUCH, ARAR	Holmes et al., 1979
	Atuel River, Argentina	1600–1960	AUCH	Cobos and Boninsegna, 1983
	Río Bueno, Chile	1929-2002	AUCH, PLUV	Lara et al., 2005
	Puelo River, Chile	1599-1999	AUCH, PLUV	Lara et al., 2008

[a]Tree species codes are those used in the International Tree-Ring Data Bank; a list is found in Appendix 1.

1.4 Aims of this study

This study focuses on a region with complex land-climate interactions and scarce instrumental data. Growing interest in the climatic history of the Southern Hemisphere over the last several decades has prompted an increasing number of studies in southern South America. However, many significant gaps remain in our understanding of the land-climate interactions governing southern Patagonia. Filling these gaps will require a longer and more complete record of regional climate than is provided by instrumental records. This study attempts to achieve a broad understanding of the basic relationships between temperature, precipitation and discharge at 52°S, while at the same time answering the following questions:

- **How can we best deal with the limited instrumental climatic and hydrological records available to us?**
- **How are streamflow and tree growth related to atmospheric circulation?**
- **What is the role of the South Patagonian Icefield in modulating discharge?**
- **Can we develop a reliable reconstruction of Río Santa Cruz streamflow for the past 2-3 centuries?**

Chapter 2 - Data and Methods

2.1 Overview

The study area is located on the eastern slope of the Andes in the *Nothofagus pumilio* forests of Parque Nacional Los Glaciares, southern Patagonia. This study focuses on sites located in two small glacial valleys (Heim and Torre) that drain directly into lakes Argentino and Viedma, respectively (Figure 2.1). The Torre valley is located above the village of El Chaltén. Three short-term dataloggers, in place since March 2002, indicate that the annual mean temperature in this region decreases from 6°C at 760 m elevation to less than 2°C at 1,100 m elevation (Srur et al, 2008). Similarly, data from the ranger station in El Chaltén (500 m a.s.l.) indicate a mean annual precipitation of 439 mm. Long-term meteorological and hydrological records for the study area are generally lacking; those that do exist do not exceed 45 years. However, *Nothofagus* forests in this region extend over a large altitudinal gradient from 500 to 1150 m a.s.l. and have been shown to reflect variations in both temperature and precipitation (e.g., Villalba et al., 1990 and 1998; Lara et al., 2001 and 2005; Aravena et al., 2002). The locations of hydrologic and meteorological stations used in this study are shown in Figure 2.1, as are the locations of the two valleys where trees were sampled.

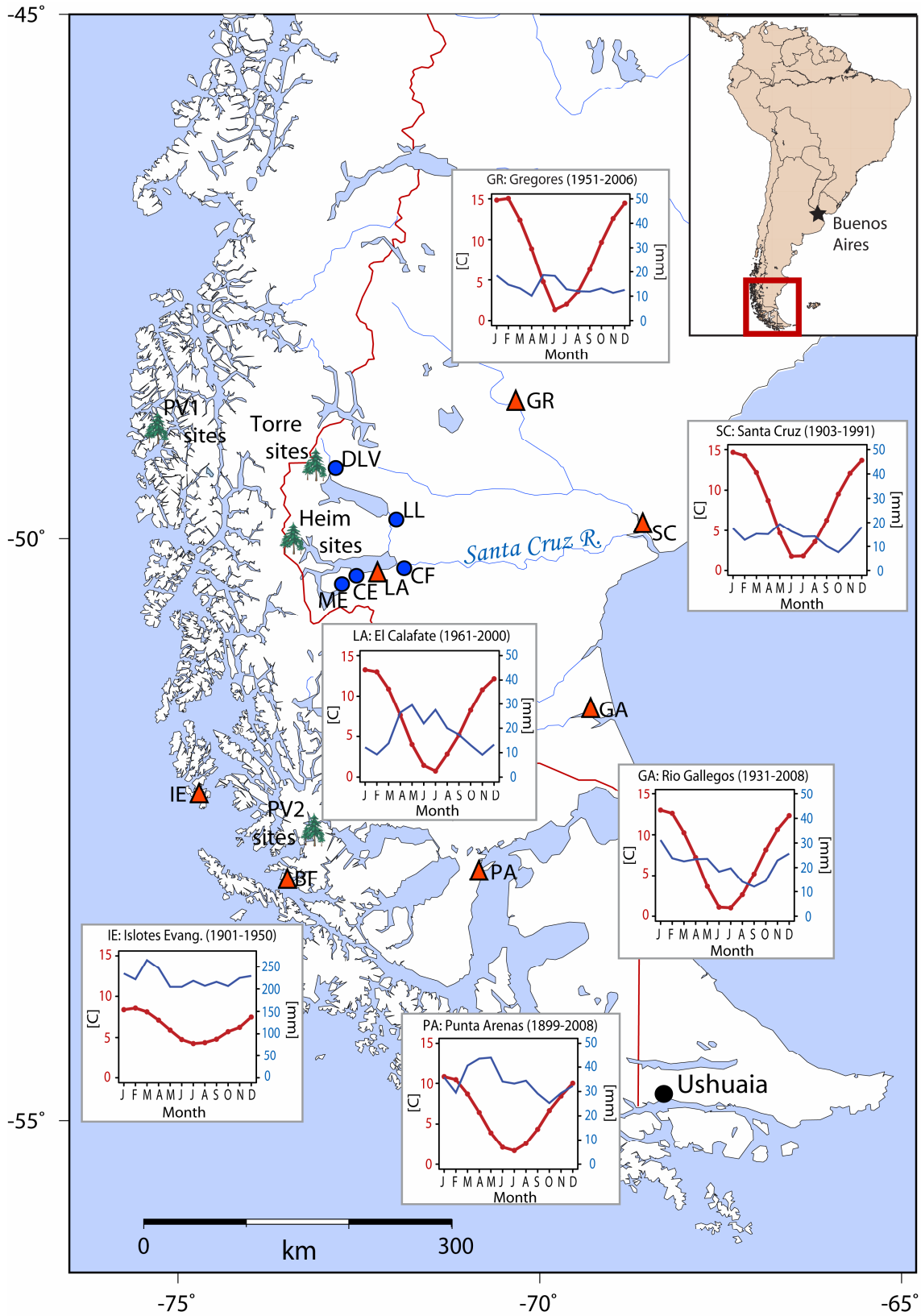

Figure 2.1. Regional map showing the location of the tree ring chronologies (tree symbols), meteorological stations (red triangles) and streamflow gauges (blue dots). Mean monthly temperature (red curves) and precipitation (blue curves) are shown for all meteorological stations except Bahia Felix, for which only precipitation data is available. Note that the temperature and precipitation scales are the same for all stations except Islotes Evangelista, which receives almost 50 times more precipitation.

2.2. Instrumental data

2.2.1. Streamflow records

Streamflow records were obtained from Argentina's Subsecretaría de Recursos Hídricos. Five streamflow records exist for the Santa Cruz basin, only two of which are longer than 15 years. The De Las Vueltas gauging station is located in Parque Nacional de los Glaciares near the town of El Chaltén. The De Las Vueltas River drains a relatively small watershed (671 km^2) before terminating in Lago Viedma (1088 km^2). Lago Viedma is linked to Lago Argentino via Río La Leona, which supplies about 35% of the total Río Santa Cruz annual discharge (Depetris and Pasquini, 2000). The Charles Fuhr hydrological station is situated on the Río Santa Cruz itself, about six kilometers from the point where Lake Argentino empties into the river. There are no dams upstream of the Charles Fuhr hydrological station, nor is there any significant industry or farming in the catchment above the Charles Fuhr gauge. Only two small towns are located in the upstream catchment: El Calafate (population ~15,000) and El Chaltén (population ~500), the economies of which are devoted almost entirely to tourism in nearby Parque Nacional Los Glaciares. The location of these stations as well two additional stations situated on small tributaries to the Santa Cruz are shown in Figure 2.1. Station details are provided in Table 2.1.

Table 2.1. Characteristics of the streamflow stations used in this study.

Station	Lat/Long	River	Area (km^2)	Mean Q (m^3/s)	Elevation (m)	Period	Missing monthly values (%)*
Charles Fuhr (CF)	50.33°S / 72.51°W	Santa Cruz	15,500	698.1	206	1956-2007	0.03
La Leona (LL)	50.41°S / 72.73°W	La Leona	7,450	250.6	250	1956-2007	25.6
De Las Vueltas (DLV)	49.34°S / 72.85°W	De Las Vueltas	671	51.4	345	1992-2007	0.06
Centinela (CE)	50.27°S / 71.88°W	Centinela	516	4.6	275	1993-2004	0.02
Mitre (MI)	49.81°S / 72.05°W	Mitre	118	4.7	200	1993-2004	0.02

*Estimated as the number of months without data divided by the total number of months included in the period indicated in the table multiplied by 100.

Two smaller rivers (Mitre and Centinela) drain the Andean foothills directly but are not connected to glaciers. As a result, their discharge more closely mirrors precipitation events and snowmelt. Both exhibit the rapid response to precipitation and melt events characteristic of small alpine streams. In contrast, La Leona and Santa Cruz exhibit discharge regimes reflecting the modulating presence of the two large lakes. Maximum mean discharge at both stations occurs in March as a consequence of snowmelt and ice ablation, about a month after maximum summer temperatures peak. A third flow regime is represented by De Las Vueltas. Like the Mitre and Centinela rivers, De Las Vueltas responds to precipitation but is most strongly influenced by meltwater from the many glaciers that drain into it. Figure 2.2 illustrates the response of the smaller, glacier-free rivers and the larger, lake-dampened rivers to precipitation and temperature, respectively.

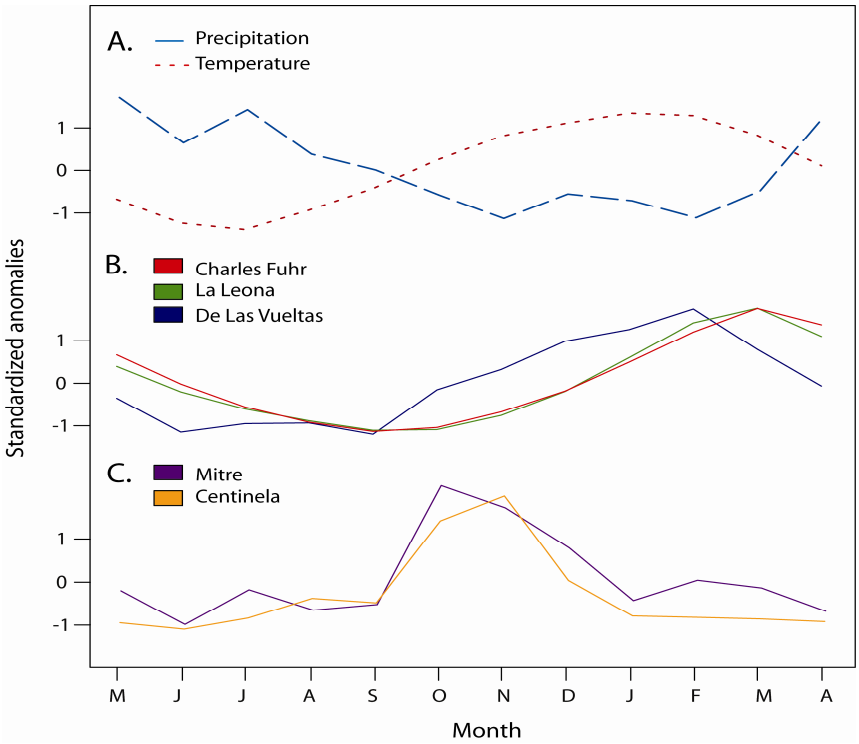

Figure 2.2. Discharge on the Río Santa Cruz and its tributaries is primarily temperature-driven (A, red line). Rising temperatures in February prompt an immediate response in the De Las Vueltas (DLV) tributary (B), where the gauge closest to the Andes is located. Peak discharge in the La Leona river (LL) and in the Santa Cruz (Charles Fuhr station, CF) river is delayed due to the buffering effect of the lakes Viedma and Argentino (B). The smaller Mitre (MI) and Centinela (CE) rivers (C), however, are not connected to glaciers and are therefore driven primarily by precipitation (A, blue line), namely snowmelt.

All instrumental data used in this study have been transformed into z-scores prior to analysis. The use of z-scores, or standardized anomalies, allows the user to work simultaneously with batches of data that are related but not strictly comparable (Wilks, 2006). The z-score allows for the direct comparison of, for example, streamflow datasets with widely varying discharge volumes and seasonal cycles. The standardized anomaly is calculated as follows:

$$Z = \frac{x - \bar{x}}{s_x}$$

Equation 1. The standardized anomaly, or z-core, is computed by subtracting the sample mean ($\bar{x}$) from the raw data (x) and dividing by the sample standard deviation (s_x).

Instrumental data used in climatic studies should be carefully reviewed for trends (e.g., Kahya and Kalayci, 2004), inhomogeneities (e.g., Alexandersson, 1986) and other non-climatic inconsistencies. However, traditional trend tests were stymied by the short time span covered by most of the streamflow records. In hydroclimatology, a period of 30 years is considered sufficient for a valid mean statistic (Kahya and Kalayci, 2004). Only the Charles Fuhr and La Leona records meet this criterion. A Mann-Kendall trend test was applied to the streamflow z-scores for both datasets. The rank-based nonparametric Mann-Kendall test (Mann, 1945; Kendall, 1975) is often used to assess the significance of monotonic trends in hydrometeorological time series because it is simple, robust and can cope with missing values. As noted by Yue et al. (2002), the main reason for using non-parametric statistical tests is that they are considered to be better suited for analysis of the non-normally distributed

data and censored data frequently encountered in hydrometeorological time series. The Spearman's rho is also used in hydrometeorological studies, but as the two tests have almost identical power, only the Mann-Kendall test was applied in this study. At a probability threshold of α=0.05, neither streamflow time series exhibited a significant trend.

Homogeneity tests such as those proposed by Alexandersson (1986) are also challenged by the amount of missing data and the short time span covered by the records. Alexandersson (1986) proposed a simple homogeneity test for precipitation based on ratios. The test assumes that the integrand precipitation amounts from nearby stations are proportional to each other. However, the widely divergent streamflow volumes and differing runoff regimes prevent the use of such a test in this study. Instead, the data were visually examined for inconsistencies, and suspected outliers (which generally precede or follow a gap in the data) were excluded. Accumulated streamflow from streams with related discharge patterns were also plotted against each other to check for step changes.

Many studies also supplement scarce instrumental data by employing gap-filling techniques (e.g., Blasing et al., 1981; Rosenblüth et al., 1997). However, hydrological records were not gap-filled for the purposes of this study, as the amount of missing data and short record spans make it difficult to establish reliable relationships. The average correlation between gauging stations over the common 1993-2003 period is 0.26. Furthermore, the gauged streams in the Santa Cruz Basin vary considerably in both runoff volume and discharge regimes (see Figure 1.4 and 2.2).

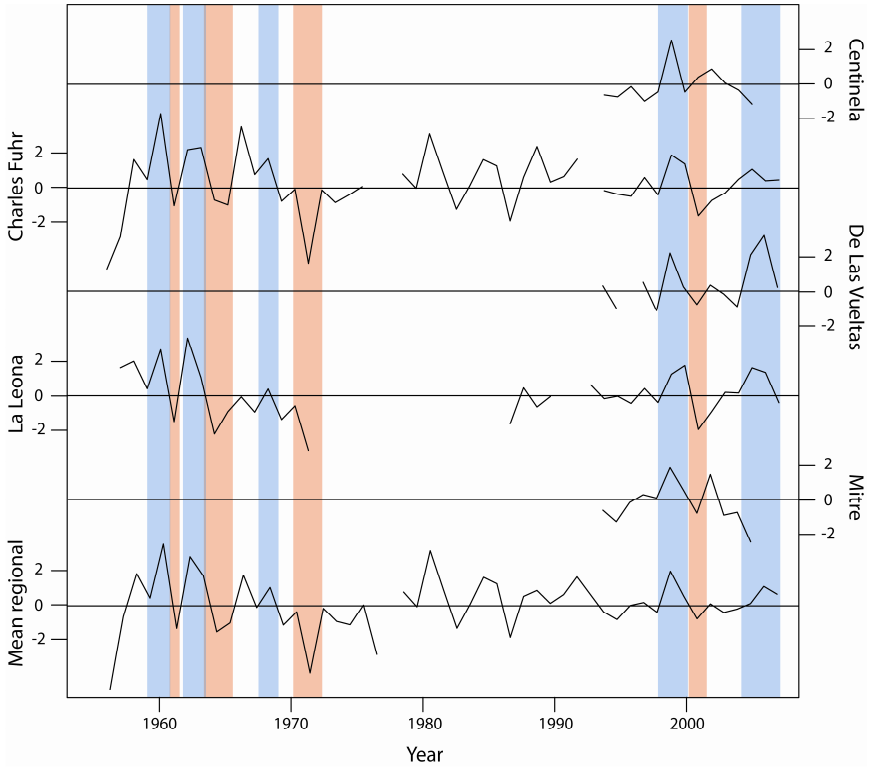

Figure 2.3. Streamflow departures for the five gauged streams in the Santa Cruz Basin. Periods of below-normal streamflow are marked with red rays, periods of above-normal streamflow are marked with blue rays. Values are unitless z-scores. The mean regional chronology includes data from all five stations.

Figure 2.3 shows annual streamflow departures for each of the five gauges in the watershed, as well as the mean departures. Standardized monthly anomalies (z-scores) were used in place of the full values for all instrumental data in this study, as the use of standardized anomalies reduces the problem of comparing station data over complex terrain and removes the seasonal signal. Streamflow departures were calculated by subtracting the long-term annual mean discharge from the mean discharge of each year, then standardized by dividing the standard deviation (i.e., z-scores). The common period used to standardize the series was 1993-2003. As the input of meltwater during the austral spring and summer (October to March) dominates the hydrological cycle, a single water year was defined as running from May 1 to April 30 following Waylen et al (2000).

As Mitre, Centinela and De Las Vueltas records are too short to meet statistical requirements and because all three are small rivers with differing flow regimes, only the two longest streamflow records (La Leona and Charles Fuhr) were used for comparison with tree-ring width. Both records were checked for inconsistencies as discussed above, normalized and then averaged to create a single discharge record for the Río Santa Cruz. The final discharge record extends from 1956 to 2007 and contains 15 months of missing data, or 2%. The agreement of the mean record with the station records can be seen in Figure 2.4. The standardized monthly anomalies of the mean discharge record correlate strongly with those of La Leona and Charles Fuhr at 0.92 and 0.91, respectively, over the 1993-2003 period common to all records. Over the full 50-year period, the correlations are only slightly different (0.92 and 0.89, respectively). The mean discharge record does not correlate significantly with the smaller De Las Vueltas, Mitre or Centinela records ($p<0.05$).

2.2.2. Meteorological records

Monthly temperature and precipitation data were retrieved from the NASA Goddard Institute for Space Sciences (GISS data) and from the Royal Netherlands Meteorological Institute's (KNMI) Climate Explorer (Global Historical Climatology Network data (GHCN)). The density of official meteorological stations in Patagonia is extremely low (approximately 30,000 km^2/station before 1950 and 40,000 km^2 in 1997 (Paruelo et al. 1998)). As a result, there is only one meteorological record in the immediate vicinity of the study area, located near the town of El Calafate. The next nearest meteorological station is located 231 km to the northeast at Gobernador Gregores. The characteristics of the meteorological stations used in this study, including the amount of missing values, are summarized in Table 2.2.

There is a considerable amount of missing data in all meteorological records used for this study. Figure 2.4 shows the normalized mean annual time series for all instrumental records used in this study. GHCN precipitation data was only available from KNMI, but both GISS and KNMI have temperature records available for all six stations. Although the difference between temperature values in the two datasets is insignificant, the GISS datasets typically contain fewer missing values. For the purposes of this study, the GISS temperature datasets were used. Whenever possible, missing values in the GISS datasets were replaced with information available in the KNMI-GHCN datasets.

Table 2.2. Summary of meteorological station characteristics.

Station name	Lat/ Long	Elevation (m)	Temp. period	Precip. period	Missing values, T (%)*	Missing values, P (%)*
El Calafate (LA)	50.3°S / 72.3°W	220	1961-2000	1961-2000	14.2	9.17
Bahía Felix, Chile (BF)	53°S / 74.1°W	15	NA	1913-1980	NA	0.01
Gobernador Gregores (GR)	48.8°S / 70.3°W	358	1950-2006	1951-2006	27.6	23.96
Río Gallegos (GA)	51.6°S / 69.3°W	19	1931-2008	1931-2008	8.8	2.24
Santa Cruz Aeropuerto (SC)	50.02°S / 68.57°W	11	1901-1991	1903-1991	18.4	19.23
Islotes Evangelista (IE)	52.4°S / 75.1°W	52	1901-1950	1899-1980	18.8	8.43
Punta Arenas, Chile (PA)	53°S / 70.8°W	37	1888-2008	1888-2008	1.3	0.62

*Estimated as the number of months without data divided by the total number of months included in the period indicated in the table multiplied by 100.

Both GHCN and GISS data are submitted to thorough quality reviews before inclusion in the GHCN or GISS databases. These reviews include preprocessing checks on source data, time series checks that identify spurious changes in the mean and variance, spatial comparisons that verify the accuracy of the climatological mean and the seasonal cycle, and neighbor checks that identify outliers from both a serial and a spatial perspective (Peterson and Vose, 1997). For the purposes of this study, a preliminary visual inspection of each series was performed on a monthly basis. Because the temperature records correlate well between stations (average correlation over the common 1961-2001 period is 0.75), individual station records were compared with nearby stations and apparent outliers, which typically preceded or followed a gap in the data, were excluded. Precipitation and temperature records were tested for trends and inhomogeneities as discussed above for the streamflow data. The results of these tests are discussed in the Results and Discussion section.

2.2.3. CRU Data

The individual station data discussed above is useful for characterizing the region. However, the records are generally short, do not cover the same time periods and contain significant gaps and trends. Thus, it was decided that gridded climate data should be used in place of station data for analyses concerning the climate-growth relationship. Monthly mean surface temperature and monthly precipitation data were obtained for the 1901-2006 period from the KNMI Climate Explorer website (Web: KNMI). Climate Research Unit datasets (CRU TS 3), which are 0.5° gridded data based on an archive of monthly values provided by weather stations around the world, were used. CRU data are produced by converting each value into an anomaly from the 1961-1990 average value for that station. Thus, each grid box value is the mean of all the station anomalies within that grid box.

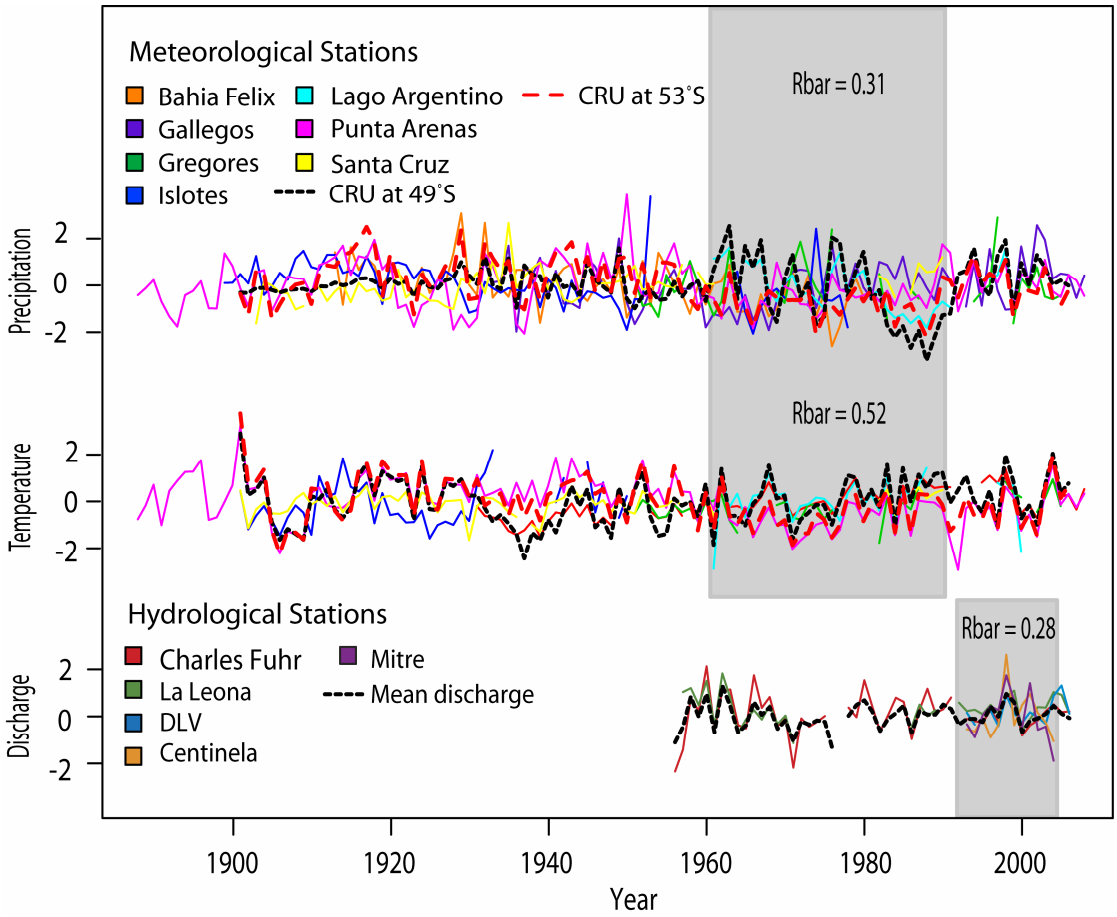

Figure 2.4. Time series of all hydrologic and meteorological data used in this study. All times series are standardized anomalies. Meteorological correlations are computed over the 30-year common interval (1961-1991), excluding Islotes and Bahia Felix whose temperature records end in 1950 and don't exist, respectively, and whose precipitation records end in 1980. The period common to the hydrological records is eleven years (1993-2003).

The use of CRU data in this study is advantageous for several reasons. CRU data is universally available and may therefore be used by other researchers working in the same region. It also eliminates inconsistencies in the manner in which researchers prepare climate data for interpretation and ensures a common level of uncertainty among different climate analyses in the same region. Furthermore, CRU data provides gap-filling that the GISS and GHCN station data do not, thereby providing complete climate records. All data used to produce the CRU datasets are first corrected for uncertainties, replication differences, biases and measurement error. Only stations with 75% or more valid monthly measurements in the reference period (1931-1970 or 1951-1990) are used to create the gridded datasets (Web: CRU). Finally, the interpolation technique for missing data is consistent: an estimate of the value is obtained by calculating the mean anomaly for that location derived from surrounding locations and then interpolated onto the missing station location using an inverse distance (with spherical adjustment), angular weighted method (Web: NCAR).

For the purposes of this study, a single averaged grid point was selected for each grouped study site and gridded 2.5 x 3.75 degree precipitation and temperature data were generated. Time series from individual grid cells between 48 and 51°S showed no significant differences, so a single dataset centered between 49 and 50°S was generated and used for all sites between these latitudes. A second CRU dataset was produced for all sites between 53

and 54°S. These data, shown in Figure 2.4 in dotted black (49°S) and dashed red lines (53°S), are in reasonable agreement with the individual station records and offer 106 years of continuous climatic information. It should be noted that when CRU data is included in the inter-station rbar calculation (1961-1991), the precipitation rbar increases slightly (from 0.29) and the temperature rbar decreases significantly (from 0.74). This suggests that there are either problems with the station data that the CRU processing addressed or that the CRU processing introduced features that are not supported in the station data. Given the inconsistencies observed in the station data, it is assumed that the CRU processing is correct and that the CRU data are more representative of the regional climate than the individual station data.

2.3. Dendrochronology
2.3.1. Sample collection

Increment cores from living *Nothofagus pumilio* trees were collected in the headwaters of the Río Santa Cruz in Parque Nacional Los Glaciares during the austral summer of 2007. Three annual tree-ring index chronologies were developed for each of two valleys containing large glaciers that drain directly into the lakes that give rise to the Río Santa Cruz. The Torre valley is located above the village of El Chalten. Trees were sampled on either side of the valley flanking Glaciar Grande (also known as Glaciar Torre), which terminates in Laguna Torre. The lake drains into the Fitz Roy River, which is quickly intercepted by the De Las Vueltas River. Both sites are located near cold tree line and are expected to be sensitive to temperature. A third site is located on an old end moraine along the Torre valley and should also be temperatures-sensitive. The Heim valley is located in the southern end of the Upsala branch of Lake Argentino. The Heim valley is a much narrower valley than the Torre valley and drains almost immediately into Lake Argentino. Trees were sampled, as before, on either side of the valley flanking Glaciar Heim at tree line and on an old end moraine located in the valley below the glacier. The site characteristics for each chronology are summarized in Table 2.3.

As noted above, the sampling sites are situated on the slopes and moraines flanking large glaciers that terminate in lakes. All sites except Torre Morena 4 and Heim Morena 4 are located close to high tree line on moderately steep, well-drained slopes. Forest stands selected for sampling were chosen such that natural (i.e., avalanches, debris flows) and human disturbances (i.e., timber harvesting, trail development) were avoided. It should be noted that the altitudinal proximity of cold and dry tree line in southeastern Patagonia makes careful site selection especially important. Trees growing on the well-drained slopes typical of a glacial setting on the lee-side of the Andes may be stressed by both moisture and temperature at the high tree line. Similarly, trees exposed to the cold, dry winds blowing off the glaciers may show a mixed signal. Care was taken to ensure that sites selected for this study respond predominately to a single climatic signal.

Table 2.3. Site characteristics of tree-ring records included in the composite chronologies.

Site Code	Site Name	Description	Elevation (m)	No. Trees	No. Radii
TN	Torre Norte	North-exposed slope above front end of glacier; steep slope; sparse, dry undergrowth	921	21	42
TS	Torre Sur	South-exposed slope above front end of glacier; slightly below krummholz; steep slope; humid site with ferns	855	23	50
TM4	Torre Morena 4	End moraine at eastern shore of Laguna Torre; east slope of moraine (opposite slope is bare)	658	22	54
HCO	Heim Cronología Oeste	Left margin of glacier, SSE-facing slope; mixed coihue, lenga; steep slope; old moraines evident; sparse undergrowth	496	23	57
HME	Heim Morena Este	On NNW-facing slope above glacier; humid site below krummholz; mixed coihue, lenga; wild cows	650	20	43
HM4	Heim Morena 4	Right margin of glacier; sampling along moraines 2-4; less steep; undergrowth prevalent but seldom shrubby; mixed coihue, lenga	426	25	52

To ensure adequate sample replication, a minimum of two radii were extracted from each of twenty or more trees (Fritts, 1976). Trees were sampled at breast height using a classic increment borer (Haglöf, 20 inch length, 5mm diameter). Increment corers extract a pencil-sized sample of wood from the trunk, allowing the annual rings of the tree to be examined without harming the stem. The cores of each site were labeled, placed in core holders (straws), and air-dried immediately upon reaching the laboratory to prevent decay (Schweingruber, 1988). Since the biological growth season in the Southern Hemisphere does not coincide with the calendar year, Schulman's convention (1956) was adopted and the date of the annual ring was assigned to the year when ring growth began.

2.3.2. Sample preparation and measurement

Initial sample preparation took place in the dendrochronology laboratory of the Instituto Argentino de Nivología, Glaciología y Ciencias Ambientales in Mendoza, Argentina. All remaining sample preparation and measurement was carried out in the Dendro Sciences laboratory of the Swiss Federal Research Institute (WSL) in Birmensdorf, Switzerland. Once the cores were fully dry, they were mounted on pregrooved sticks with their fiber direction perpendicular to the mount using water-soluble glue (Fritts, 1976). The samples were fixed in place with masking tape to prevent the cores from shifting during the drying process.

Once dry, the cores were polished using a belt sander. Although a microtome can often be used to render the annual rings of wood samples visible, the fine, ring-porous nature of *N. pumilio* made obtaining a clear surface very difficult. Instead, the cores were polished with an increasing sandpaper grit count (180, 320, 400). When necessary, the samples were polished further by hand with 800-grit sandpaper. The sanding process pushes wood dust into the lumen, which allows for a better contrast between the dark cell wall and the lighter (dust-filled) cell-cavity (Schweingruber, 1988).

Relative and absolute measurements of annual ring width are the most common climate proxies originating from trees and depend on accurate dating. First, rings are visually dated using a binocular microscope. Using a pin or a soft-leaded pencil tip, decades are marked using a system of dots in which one dot signifies a decade, two dots indicate a half-century and three dots denote a full century. This decade-marking method simplifies the dating and measuring process significantly as it reduces the potential for error and makes tracking missing rings, false rings or simple dating errors much easier.

Once the cores have been dated, absolute ring-width measurements are obtained using a LINTAB^{TM}-5 measurement station and the associated TSAP-WIN^{TM} software (Web: Rinntech). The distance from one ring boundary to the next is measured as the program registers the manually steered movement of the measurement table. The cross-hairs in one ocular allow the user to mark the rings by mouse-click or foot pedal while the sample attached to the measurement table is moved continuously underneath the microscope. Thus, a series of absolute ring width measurements [1/100 mm] for each core are recorded and stored in TSAP, where they can be adjusted to account for missing or false rings during the crossdating process.

2.3.3. Crossdating and detrending

Annual tree rings are formed in most perennial woody plants growing in regions characterized by pronounced seasonality. Annual climatic fluctuations (i.e., warm and cold, wet and dry) result in cyclic periods of growth and dormancy that are recorded in annual increments of xylem. However, ring structure may vary greatly depending on the occurrence of extreme events such as avalanches, debris flows and insect outbreaks or changes in external parameters such as light, moisture and temperature. During a year of extreme climate a tree may not form a ring on all portions of the stem, resulting in a missing ring in the core sample. At other times, changes in cell structure will occur within an annual growth increment resembling the boundary of a true annual ring (Fritts, 1976). These missing and false rings complicate the dating process because the presence or absence of rings in the wrong place leads to an incorrect age assignment.

Crossdating, however, ensures the proper placement in time of each growth ring. Crossdating functions on the concept of limiting factors, which is the observation that populations of trees exposed to similar limiting conditions will produce synchronous variations in ring structure (Fritts 1976). Thus, ring-width series from all radii within a stem should reflect a common pattern that is in turn shared with different trees in a given stand, as well as among ring-width patterns of neighboring stands. The samples used in this study were crossdated by first comparing growth curves of cores from the same tree, then comparing cores of different trees within the same site. Crossdating was verified and corrected with the help of the computer program COFECHA, a quality-control program used to check the crossdating and overall quality of tree-ring chronologies (Holmes, 1983). COFECHA compares segments of a definable length and points out those parts of a series that are not in agreement with the corresponding parts of other series (Holmes, 1983). Thus, false rings and missing rings may be detected and accommodated in order to generate a reliable, accurately dated chronology.

Using the Auto-Regressive Standardization program (ARSTAN; Cook and Holmes, 1986), the crossdated measurement series were standardized to remove the biological age trend and retain the majority of the climate-related variance. Given the relatively short chronologies available and the fact that a majority of the trees display weak age trends (due perhaps to the fact that few cores contain the center), several different detrending methods were explored. All series were detrended using variance stabilized 200-, 100 -and 32-year splines, as well as Regional Standardized Curves (RCS) and by fitting a standard negative exponential to the series. The resulting standardized chronologies were then correlated with temperature, precipitation and discharge records to determine which detrending method best captures the tree growth-climate relationship.

After comparison with climatic data, a conservative, 200 year cubic spline detrending method was chosen to retain as much low frequency variation as possible, as the trees are expected to be most sensitive to longer-term changes in water availability. In ARSTAN, the amount of variance to be removed at a particular frequency is specified as the 50 percent cutoff wavelength (Cook and Peters, 1981). Thus, a 200 year cubic spline preserves most of the variation at wavelengths of 100 years or less. The measured ring-width values were divided by the values predicted by the curve for each year, producing stationary, dimensionless ring width indices with a mean of 1 and a constant variance (Cook, 1987). Finally, a robust weighted mean was used to combine all series into a single site chronology. The biweight robust mean discounts the influence of extreme values by using the arithmetic mean or

median as the initial estimate (Cook, 1985) and therefore removes the effects of endogenous stand disturbances.

The agreement between series within each chronology was assessed using running series of Rbar and expressed population signal (EPS) statistics (Briffa, 1995). Rbar is the mean correlation coefficient of all possible pairings among tree-ring series from individual cores, computed for a specific common interval (Briffa, 1995). A 50-year window with a 25-year overlap was used. EPS is a measure of the similarity between a chronology and a hypothetical chronology that has been infinitely replicated (Briffa, 1995) and is used to evaluate the weakening representation of the chronology due to decreasing sample size back to the past. A function of the average correlation between trees (Rbar) and sample depth, an EPS value of 1 indicates an ideal chronology (Equation 2). An EPS value of 0.85 is a widely accepted threshold for adequate sample size in chronology development; however, to simplify the programming demands of this study, chronologies were simply truncated when sample size reached 10. For the samples used in this study, an EPS value of 0.85 is reached or exceeded when n=10.

$$EPS(t) = \frac{n * Rbar}{n * Rbar + (1-Rbar)}.$$

Equation 2. The Expressed Population Signal is a function of the mean correlation coefficient (Rbar) and the sample size (n). A value of 0.85 is commonly accepted as the threshold value for a valid sample size (Wigley et al., 1986). Because a sample size of ten is roughly equivalent to an EPS of 0.85 for the chronologies developed in this study, a sample size of ten was used instead of the EPS for simplicity.

Table 2.4 gives the descriptive statistics for the six *Nothofagus* tree-ring chronologies developed in this study. As described in the following section, these chronologies were later combined into composite chronologies in order to better capture the common growth patterns from each region.

Table 2.4. Descriptive statistics for the six standard (not prewhitened) *Nothofagus pumilio* tree-ring chronologies developed in this study.

Site code	Period of record	No. of series	Mean tree-ring width (mm)	Mean sensitivity*	1st-order autocorrelation[đ]	Rbar[Ψ]
TS	1674-2007	46	0.79	0.246	0.696	0.572
TN	1669-2007	35	1.01	0.285	0.715	0.550
TM4	1703-2007	42	1.08	0.273	0.623	0.637
HCO	1741-2007	35	1.16	0.253	0.562	0.549
HME	1684-2007	33	1.33	0.259	0.663	0.557
HM4	1715-2007	33	0.97	0.236	0.670	0.541

*Mean sensitivity is the measure of the relative changes in ring width variations from year to year (Fritts, 1976).
[đ]Autocorrelation is the serial correlation coefficient for the chronology at a lag of 1 year.
[Ψ]Rbar is the mean correlation coefficient for all possible pairings among tree-ring series from individual cores, computed for a specific common time interval. A 50-year window with a 25-year overlap was used in this study (Briffa, 1995).

2.3.4. Developing regional chronologies

In order to better capture the common growth patterns for each region, composite chronologies were created by combining the individual site chronologies with the highest correlations (≥0.6). The Torre Sur (TS) and Torre Norte (TN) chronologies were therefore combined, as were the Heim Cronología Oeste (HCO) and Heim Moraine 4 (HM4) chronologies. In addition, several chronologies contributed by other researchers were included. A *Nothofagus* chronology developed in a nearby valley, Glaciar Piedras Blanca (GPB), correlates well with the Torre Norte and Torre Sur sites and was therefore included in the Torre group (chronology contributed by Ricardo Villalba).

Two *Pilgerodendron uviferum* chronologies from approximately 48.7°S / 73.9°W and 53.7°S / 71.8°W were contributed by Juan Carlos Aravena. Both of these chronologies (PV1 and PV2) combine many individual site chronologies with similar characteristics into a single chronology reflecting the mean climate response. Although a different species, the *Pilgerodendron* chronologies were used because they provide information about climatic conditions on the western slope of the Andes. *P. uviferum* occupies a wide geographical distribution between approximately 40°S and 56°S, occurring primarily in Chile but also in small stands in western Argentina. This species generally forms coastal forests or open stands in sheltered lowland bogs further inland at 0-150 m above sea level, although it may also be found at elevations up to 1000 m in both Chile and Argentina (Roig et al., 2008). At its southern extent, growth of *P. uviferum* is primarily affected by annual temperature (Roig and Boninsegna, 1990). The *Pilgerodendron* samples used in this study were collected at the same latitude as the *Nothofagus* samples and provide a more thorough understanding of climate conditions on either side of the Andes.

The descriptive statistics for the four regional standard tree-ring chronologies are given in Table 2.5. These composite datasets were analyzed and detrended as discussed above for the individual site chronologies. In contrast to the individual site chronologies, the regional chronologies were truncated where sample size (>20). This was done to ensure adequate representation of the sites used in each regional chronology. The combination of individual site chronologies to create regional chronologies with high sample replication and robust rbar statistics is advantageous because it captures the common growth signal from each region (Lara et al., 2005) and reduces the influence of site-specific noise, such as proximity to a glacial microclimate.

Table 2.5. Descriptive statistics for the regional standard tree-ring chronologies developed in this study.

Site code	Sites included	Period of record	No. of series	Mean tree-ring width (mm)	Mean sensitivity*	1st-order autocorrelation[d]	Rbar[Ψ]
Torre	TS,TM4,GPB	1629-2007	126	1.20	0.264	0.698	0.525
Heim	HM4,HCO	1715-2007	67	1.06	0.244	0.619	0.540
PV1	multiple	1370-2004	162	0.36	0.219	0.766	0.473
PV2	multiple	1371-2003	205	0.64	0.216	0.778	0.518

*Mean sensitivity is the measure of the relative changes in ring width variations from year to year (Fritts, 1976).
[d]Autocorrelation is the serial correlation coefficient for the chronology at a lag of 1 year.
[Ψ]Rbar is the mean correlation coefficient for all possible pairings among tree-ring series from individual cores, computed for a specific common time interval. A 50-year window with a 25-year overlap was used in this study (Briffa, 1995).

2.4. Age-growth relationships

Due to the prevalence of fungal infection, neither pith measurements nor pith offset estimates are available for the majority of trees. Of the 224 cores used in this study, less than 10% show any evidence of being close to the tree's center and even fewer actually contain pith. To obtain a reasonable estimate of the growth trends for each site, all tree ring series were combined into two groups, one composed of the six individual chronologies and one of the four composite chronologies. Each group was then detrended *en masse* using Regional Curve Standardization (RCS), then re-divided back into the appropriate individual or composite site. A single site chronology was calculated for each site by computing the mean ring width for each year. The sites were then plotted by cambial age and chronological age, thereby provided a means of evaluating the age trend and growth rate for each site despite the limitations of the data. The regional chronologies were similarly processed to obtain relative estimates of growth rates and age trends.

Although RCS is more appropriate for large, multi-centennial tree-ring chronologies that include a range of living and dead material, it is useful here for determining first-order age-growth relationships. RCS aligns individual tree-ring series by cambial age and assumes that such "age-aligned" time series describe the overall age-related growth trend for a given species in a given region (Esper et al., 2003). Thus, despite the relatively short chronologies available in this study and the lack of pith off-set information, these collectively detrended chronologies provide first-order understanding of site-specific age-related growth trends. The results and limitations of this method will be discussed further in 3.2.1 and 3.2.2.

2.5. Climatic influences on radial growth

To identify temporal associations between regional climate and *N. pumilio* radial growth, the prewhitened chronologies were correlated with monthly mean temperature, precipitation and discharge records. For this purpose, the mean discharge record derived from the standardized anomalies of the La Leona and Charles Fuhr streamflow records was used, as well as the CRU temperature and precipitation datasets for 49 and 53°S. In southern Patagonia, the growing season extends from approximately November to March. As radial tree growth is influences by climatic conditions preceding ring formation (Fritts, 1976), the previous and current growing seasons were included in the analysis. Ring width was also correlated with conditions two years previous to growth, as the trees sampled in this study are located near glaciers microclimates may influence the memory effect of the trees.

In order to determine whether the instrumental data has any first-order relation to the large-scale climate patterns governing the region, records of the Antarctic Oscillation and the Multivariate ENSO Index were downloaded from the CPC website (CPC, 2009). The indices were compared with the monthly anomalies of the instrumental records. The Antarctic Oscillation (AAO) is the dominant mode of climate variability at mid- to high latitudes in the southern hemisphere (Thompson and Wallace, 2000). The positive state of this annular mode is associated with strong polar lows and intensified subtropical highs centered at about 40-50°S, a latitudinal range that encompasses the study area. This pressure gradient drives a strong extratropical circulation that strongly influences temperature and precipitation in southern South America (Villalba et al., 2007)

The El Niño/Southern Oscillation (ENSO) also plays a key role in the climate variability of southern South America at this latitude. The most important coupled ocean-atmosphere phenomenon causing global climate variability on interannual time scales, changes in ENSO are tracked by the Multivariate ENSO index, or MEI. The MEI is a weighted average of the main ENSO features: sea-level pressure, the zonal and meridional components of the surface wind, sea surface temperature (SST), surface air temperature, and total percent cloudiness (CDC, 2009).

Chapter 3 - Results and Discussion

3.1. Climate and discharge relationships

3.1.1. Temperature station data

The data from the six meteorological stations employed in this study represent most of the climatic information available between approximately 46°S and 53°S. However, they straddle both sides of the Andes and therefore provide a fairly representative image of the main climatic patterns governing southern Patagonia. As noted in the introduction, a strong west to east climatic gradient exists in southern South America as a result of the prevailing winds from the Pacific colliding with the western slope of the Andes. The meteorological stations in this region include two stations (Islotes Evangelistas and Bahia Felix) located on the west side of the Andes. Temperature data are not available for Bahia Felix, but the modulating influence of the Pacific Ocean, which results in fairly stable temperatures throughout the year, can be seen in Figure 3.1. A third station, Punta Arenas is located further inland and reflects a transitional zone between maritime and continental climate regimes.

In contrast, the stations located on the east side of the Andes exhibit greater annual and diurnal temperature variations in keeping with their more continental climates. Temperatures peak in January and February whereas temperature minimums occur in June and July. At the El Calafate meteorological station, monthly temperatures range from approximately 1°C in July to 13°C in January. This temperature range is more pronounced at the more northerly stations (Santa Cruz and Gregores) and decreases toward higher latitudes (Gallegos and El Calafate), where the Andes lose altitude and the topography is increasingly dominated by fjords and lakes. It should be noted that both Gallegos and Santa Cruz are situated on the Atlantic Coast and therefore influenced to some extent by the ocean.

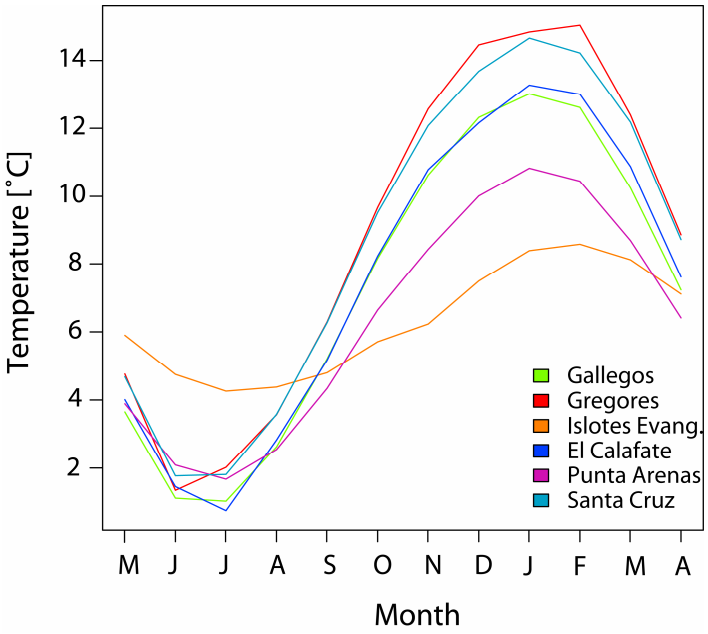

Figure 3.1. Mean monthly temperatures at each station over each station's period of record (see Table 2.2). A clear increase in temperature variability is evident as one moves west from Islotes Evangelista on the Pacific coast to Gallegos and Santa Cruz on the Atlantic coast. Similarly, temperature variability tends to increase with decreasing latitude. Temperature data are not available for Bahia Felix.

The slight increase in surface temperature over the last century that has been noted for southern South America (Rosenblüth et al., 1995; Rosenblüth et al. 1997; Jones et al., 1986) is also observed in several of the records used in this study. Figure 3.2 gives a visual impression of annual temperature trends at each station over their entire period of record. These trends illustrate the difficulty of working with station data in this part of the world. All records are short and contain a considerable amount of missing data. It is possible that some of the trends would be less extreme if the data gaps were filled. However, in spite of these limitations, an interesting geographical trend is evident. The westernmost and central stations (Islotes Evangelista, El Calafate and Santa Cruz) maintain a small but positive temperature trend throughout their period of record. As one moves eastward, the temperature trend increase becomes more pronounced (Gallegos and Gregores). Punta Arenas stands out as an exception due to a small but consistent decreasing temperature trend. Mann-Kendall trend tests, which are a function of the ranks of the observations rather than their actual values, indicate that these trends are significant at the α=0.05 level for all stations except El Calafate and Santa Cruz.

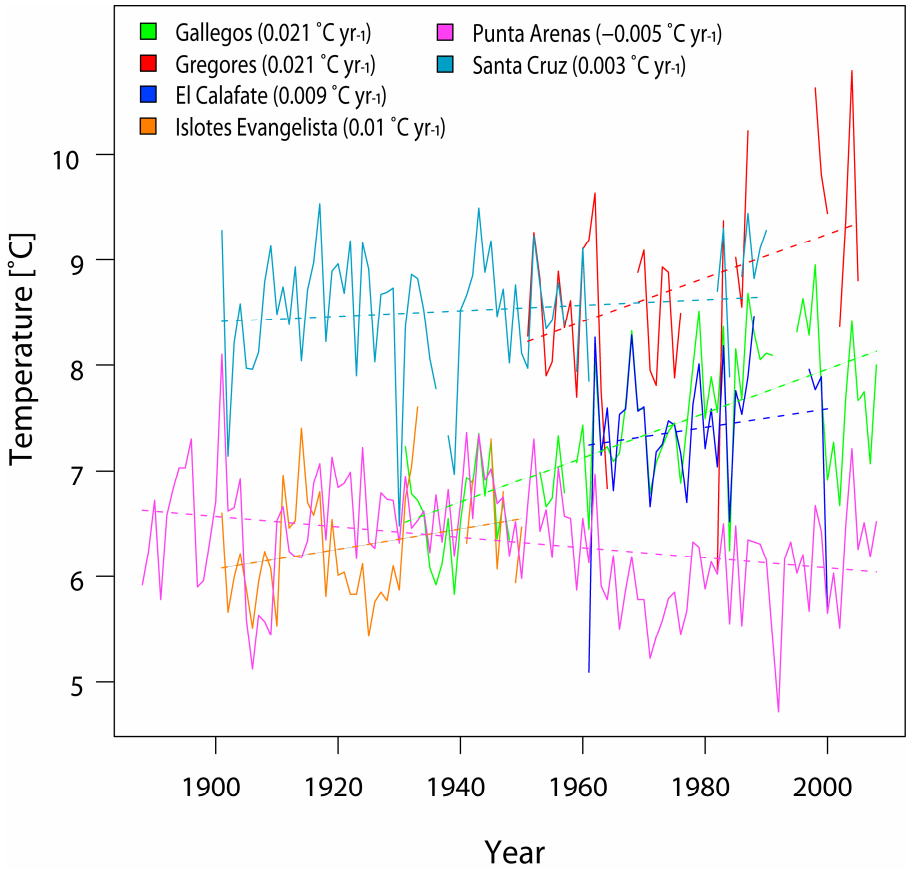

Figure 3.2. Annual mean temperature* at each station over the period of record (refer to Table 2.2). Note the increasing trend at Gallegos and Gregores, mostly stable temperature trends at Lago, Islotes Evangelistas and Santa Cruz, and a slightly decreasing temperature trend at Punta Arenas.
*Annual mean is calculated only for years with 9 or more months of data.

The temperature trend exhibited by all but one of the stations in this region suggests that the region as a whole may be experiencing a long-term warming trend, an observation that has been noted by other workers in southern South America (see above). Inter-station correlations indicate that the stations experience a common temperature signal, despite the

distances and topographical barriers separating them. All inter-station correlation coefficients exceed 0.68 ($p < 0.05$) over the thirty years common to all stations except Islotes Evangelistas (the Islotes record predates the other records, Table 3.2).

Table 3.2. Correlations between monthly anomalies at all stations for the common period 1961-1991. Islotes Evangelistas and Bahia Felix are not included because the records predate the common period. Red indicates temperature correlations; blue indicates precipitation correlations.

	GA	GR	LA	PA	SC
GA	---	0.36	0.20	0.51	0.48
GR	0.76	---	0.43	0.18	0.39
LA	0.77	0.78	---	0.22	0.18
PA	0.75	0.71	0.75	---	0.23
SC	0.77	0.77	0.70	0.68	---

3.1.2. Precipitation station data

In contrast to the temperature data, the average correlation between precipitation records is not significant at the 95% level. The stations in the closest proximity to one another have moderately significant correlations, such as Punta Arenas and Gallegos, but the region as a whole does not experience a common precipitation signal. Similarly, stations located in climatically similar regions, namely Bahia Felix and Islotes Evangelistas on the Pacific Coast, are only slightly significantly correlated over their common period (1913-1980, $p < 0.05$). Such low precipitation correlations are indicative of both the natural variability of precipitation in a highly diverse topographic region and the sparse network coverage.

The east-west gradient is particularly pronounced in the precipitation data. Mean annual precipitation at the westernmost station, Islotes Evangelistas, exceeds 2230 mm/year. Further south and located in a large fjord, Bahia Felix receives as much as 3870 mm/year. At the same latitude but further inland, Punta Arenas receives approximately 340 mm/year and mean annual precipitation at El Calafate, the station closest to the study area, is only 180 mm/yr.

As with the temperature data, the precipitation station records were checked for trends despite the acknowledged uncertainties inherent in short, discontinuous time series. Figure 3.3 illustrates the disparate coverage of the seven precipitation stations as well as the trends found over their individual periods of record. The three easternmost stations (Islotes Evangelistas, Bahia Felix and El Calafate) exhibit notable downward trends over their periods of record. Santa Cruz and Gallegos, both located on the Atlantic coast, show a slight increase in precipitation, perhaps due to an increase in humidity resulting from warmer temperatures. Precipitation at the centrally located stations (Gregores and Punta Arenas) remains stable throughout their periods of record. Mann-Kendall trend tests indicate that these trends are significant at $\alpha=0.05$ for all stations except Gregores and Punta Arenas.

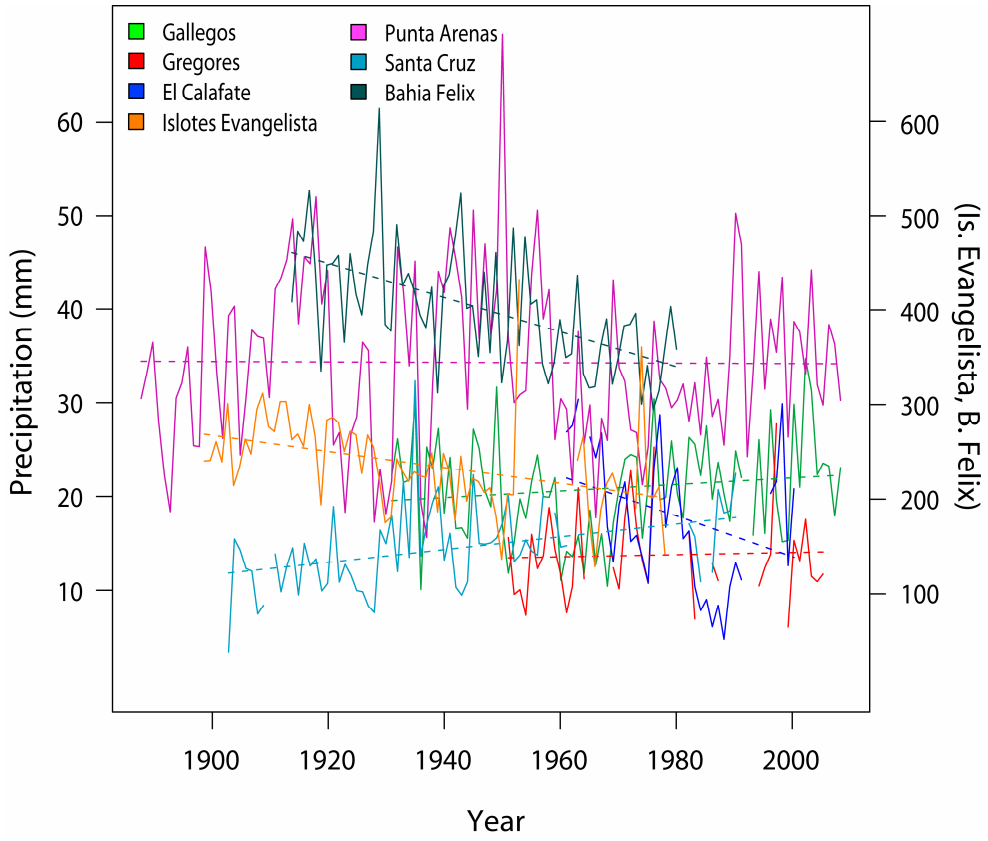

Figure 3.3. Annual mean precipitation* at seven stations in southern South America over the period of record. Precipitation at Islotes Evangelista and Bahia Felix is scaled on the right, as it is much greater than that of the other five stations. Note the decreasing trend at Bahia Felix, Islotes Evangelistas and El Calafate. The other stations have fairly flat trends over their period of record.
*Annual mean is calculated only for years with 9 or more months of data.

3.1.3. Discharge station data

Although all five hydrological stations used in this study are located within the upper Santa Cruz basin, they show a dichotomous relationship. Discharge on the La Leona and Santa Cruz (Charles Fuhr station) rivers is strongly correlated ($p < 0.05$). Both stations are located on big rivers immediately downstream from large, glacier-fed lakes (Lago Viedma and Lago Argentino, respectively). Peak flow on the Santa Cruz and La Leona rivers occurs in March, lagging slightly behind the peak summer temperature (see Figure 2.2). Centinela and Mitre, two much smaller rivers that drain out of the foothills of the Andes and are not glacier-fed, exhibit a very different pattern. Peak flow on these rivers occurs in October and November. Discharge on the smaller rivers is much more variable than the smooth mean discharge curves of Charles Fuhr and La Leona, likely reflecting a more immediate response to precipitation and snowmelt. Finally, De Las Vueltas shares similarities with both the larger and the smaller rivers. De Las Vueltas receives input from glacial melt as well as rainfall and snowmelt. Peak discharge closely follows temperature but precipitation-induced variability is also evident. As a result, although De Las Vueltas does not correlate significantly with any of the rivers, it has a weak mean correlation of 0.20 with the larger rivers and a slightly stronger correlation of 0.32 with Centinela and Mitre.

3.2. Gridded data and a combined Santa Cruz streamflow record

Two different time series drawn from the gridded CRU dataset were used for the regional temperature and precipitation records, one encompassing 53 and 54°S, the other 49 and 50°S. As discussed in Data and Methods, these datasets compare well with the individual station records and provide 106 years of complete data. To obtain a long streamflow record for the Río Santa Cruz with as little missing data as possible, the standardized streamflow anomalies of Charles Fuhr and La Leona were averaged to provide a single data set. These records were used for comparison with the tree ring data, which will be discussed in greater detail in the following sections.

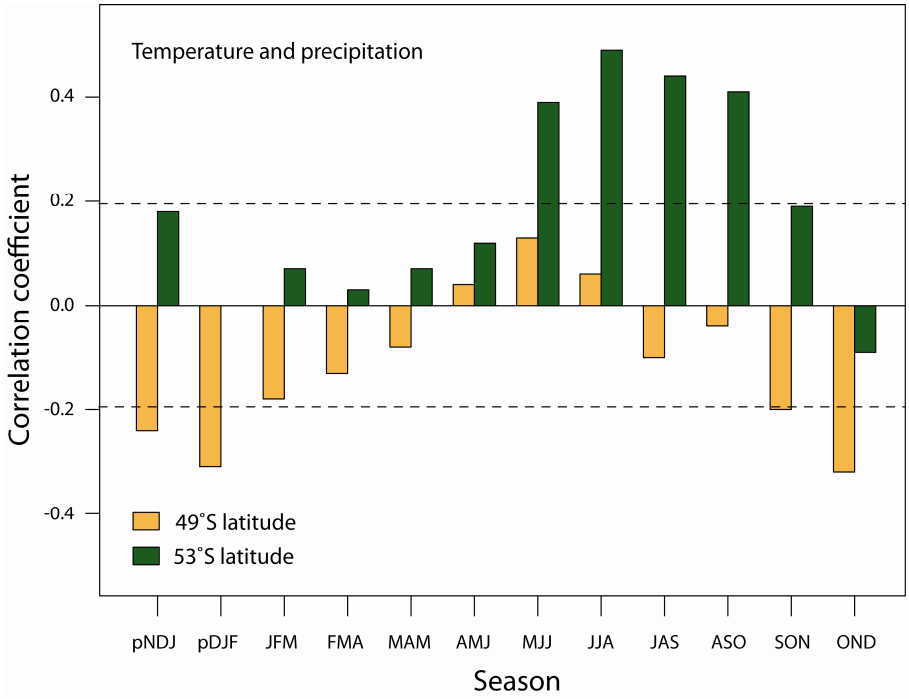

Figure 3.4. Correlations between temperature and precipitation at 49 and 53°S (1901-2006). At 49°S, temperature and precipitation are significantly negatively correlated during the summer months (November-February); at 53°S, they are positively correlated during the late fall and winter months (May-September). Dashed horizontal lines indicate statistical significance at the 95% confidence level.

Correlations between the averaged discharge dataset, the two precipitation records and the two temperature records indicate a largely temperature-dominated system. At 49°S, temperature and precipitation are significantly negatively correlated during the summer months, October through February (Figure 3.4). A weak seasonal signal exists, with positive values occurring during the fall and winter and increasingly negative correlation toward summer. The opposite behavior is observed further south. At 53°S, temperature and precipitation are significantly positively correlated from May to September. In contrast to 49°S, where the majority of precipitation falls during the winter, precipitation is highest during the summer season at 53°S (Schneider et al., 2003; Prohaska, 1976). Weak positive or negative correlations exist during the remainder of the year. The difference in precipitation timing at the two latitudes explains the opposite temperature-precipitation correlations observed in Figure 3.4.

The mean discharge record and precipitation at 49°S exhibit low but significant correlation during winter and early spring (June-August), particularly when discharge lags precipitation

by one month (Figure 3.5 a-b). The majority of precipitation falls between approximately April and July, so a positive precipitation-discharge relationship is expected over this period. However, much of this precipitation falls as snow and the discharge-precipitation relationship is therefore dependent on spring and summer temperatures. In addition, the majority of precipitation contributing to discharge falls as snow over the South Patagonian Icefield, for which precipitation records do not exist. The discharge record is therefore tightly linked to meltwater derived from the icefield, which may have been stored as snow or glacier ice for years or even centuries.

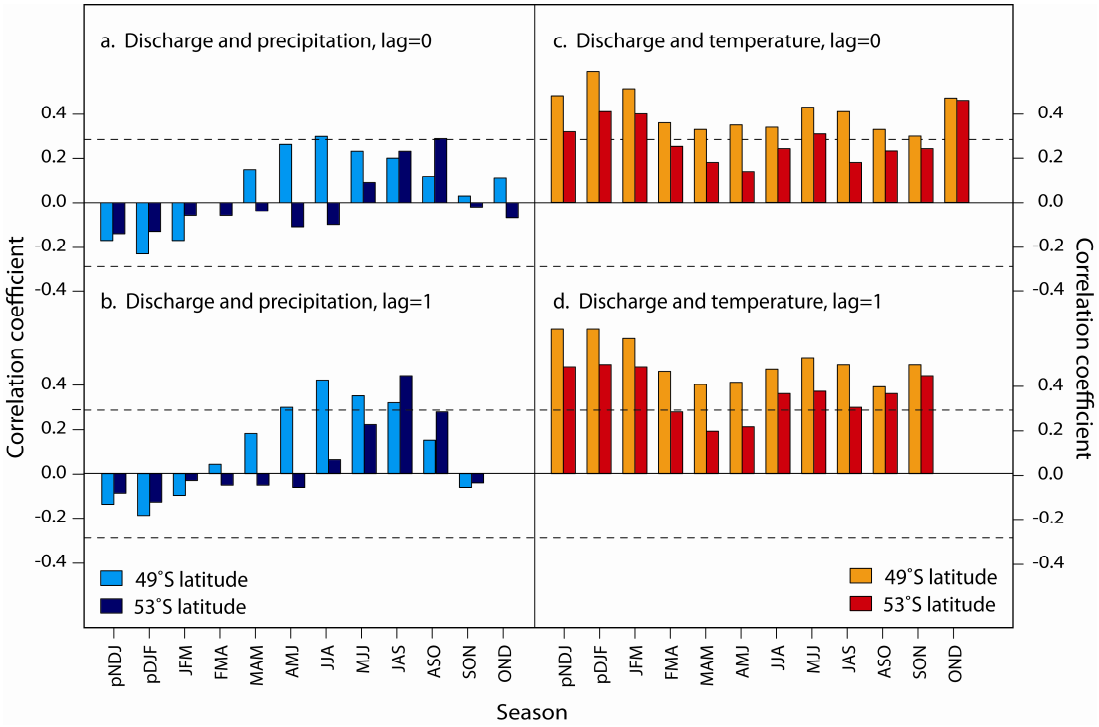

Figure 3.5. Correlations between discharge and precipitation (a-b) and discharge and temperature (c-d) at 49 and 53°S. The bottom graphs (b and d) show the relationship when temperature and precipitation are correlated with the discharge of the following month. A weak relationship exists between discharge and precipitation; in contrast, discharge and temperature are significantly correlated throughout the year, particularly at a one-month lag. Dashed horizontal lines indicate statistical significance at the 95% confidence level. Correlations are over the 1956-2006 interval.

The significance of this precipitation-temperature-discharge relationship is apparent in Figure 3.5. As noted previously, discharge lags temperature by one month or, phrased more accurately, rising temperatures in the Andes prompt a release of meltwater that is recorded by the downstream stations the following month. Temperature and discharge are positively and significantly correlated with a one-month lag throughout the year at 49°S and for most of the year at 53°S. Correlations peak in December (December temperature, January discharge) and decrease in a stepwise fashion until May. Correlations increase again through the winter, reflecting a common minimum in discharge and temperature. At 53°S, this temperature-discharge relationship is also observed, although the correlations are less strong and are not significant during the fall and early winter.

Interestingly, if the records are split into 25-year intervals, the period from 1956-1980 shows particularly strong and consistent correlations between October and March at both latitudes (Figure 3.6). This relationship remains strong in the period from 1981-2006, but the

correlation strength during the winter months (June through August) increases notably. This corroborates the general positive temperature trend observed in the individual station records (section 3.1.1). All temperature records in this region of southern South America, with the exception of Punta Arenas, show a warming trend over the past fifty years. Because the Santa Cruz basin is a meltwater-dominated system, discharge is strongly dependent on temperature. An increase in annual temperature, particularly an increase in wintertime temperature, results in an increase in runoff in the short term and a reduction in the snowpack in the long term (unless warming is accompanied by increased precipitation; Barnett et el., 2007). Thus, an increase in runoff over the past 25 years strongly suggests a corresponding increase in temperature.

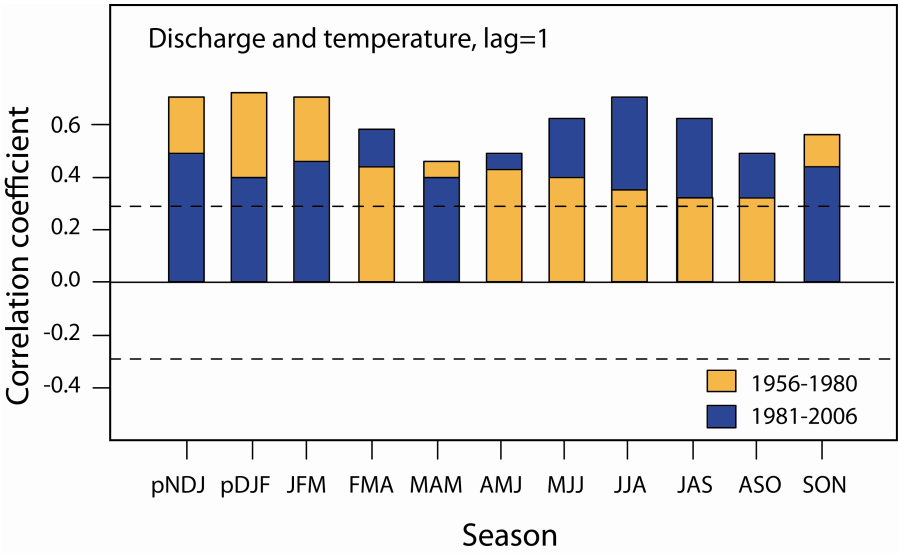

Figure 3.6. Correlations between temperature and discharge at 49°S over two different 25-year intervals and a one-month lag (1956-2006). Strengthening winter correlations suggests that the warming observed in the temperature records is reflected in the discharge record. Dashed horizontal lines indicate statistical significance at the 95% confidence level.

To determine the extent of ENSO and AAO influence on climate and discharge on the eastern slope of the Andes, MEI and AAO indices were compared to instrumental temperature, precipitation and discharge records. The positive phase of the AAO is associated with significant warming over the Antarctic Peninsula and southern Patagonia and anomalously dry conditions over southwestern South America (Thompson and Solomon, 2002). This behavior is clearly evident in Figure 3.7 (a-c): where the AAO is positively and significantly correlated with temperature, it is negatively correlated with precipitation. The strongest correlations between the AAO and temperature occur in the fall (MAM) and late spring (OND) but correlations are significant throughout the majority of the year. Similarly, a reconstruction of annual temperature variations in southern Patagonia from a network of upper-treeline *Nothofagus pumilio* chronologies shows a significant correlation with annual variations in the AAO index (Villalba et al., 2003). In contrast, AAO and precipitation show little relationship throughout most of the year. Like temperature, the strongest correlations occur in spring (~September-December), but are opposite in sign.

Interestingly, the AAO-discharge relationship is most positive when the AAO-precipitation relationship is most negative. Warmer winter and spring temperatures may be driving this positive discharge relationship but it should be noted that AAO-discharge correlations do not reflect the generally positive AAO-temperature relationship during winter. In northern

Patagonia, the summer-fall (December-May) Puelo River streamflow has been reconstructed back to 1599 (Lara et al., 2007). The study found a significant negative correlation between summer-fall runoff and the AAO, which is thought to reflect the influences of high-altitude atmospheric circulation on precipitation in northern Patagonia (Villalba et al., 2007). In this study, the correlations between summer-fall discharge and the AAO are negative but not significant, which may indicate a weaker AAO influence in southeastern Patagonia.

Correlations between the ENSO index (MEI) and the three climatic variables (Figure 3.6, d-e) are less robust. The positive phase of ENSO, or El Niño, is characterized by cold, wet winters (May-November) in southern South America; the reverse pattern occurs during the La Niña phase when the high pressure system in the southeast Pacific is strong and displaced to the south (Aceituno, 1988). While all three variables clearly oscillate with MEI over the period of record (1950-2006), only temperature at 49°S correlates significantly with MEI. Interestingly, the strongest temperature-MEI correlation occurs during the summer months (January-March). Using a mid-latitude (39-43°S) temperature reconstruction from *Fitzroya cupressoides*, Villalba et al. (2007) found that summers following El Niño episodes tend to be relatively warm and dry. Although the study area is located further south, this relationship may help to explain the positive correlation between MEI and temperature during the summer. Similarly, discharge and MEI are most strongly correlated during the summer. As noted previously, peak discharge tends to lag temperature by one month, a pattern that holds true for the MEI-temperature-discharge relationship. It should be noted that these observations are made on the basis of a single time series correlation relationship. ENSO, however, works on an interannual timescale that varies between approximately three and six years. These correlations are therefore likely to be strongly dependent on the strength of ENSO during any particular year and should be investigated more thoroughly.

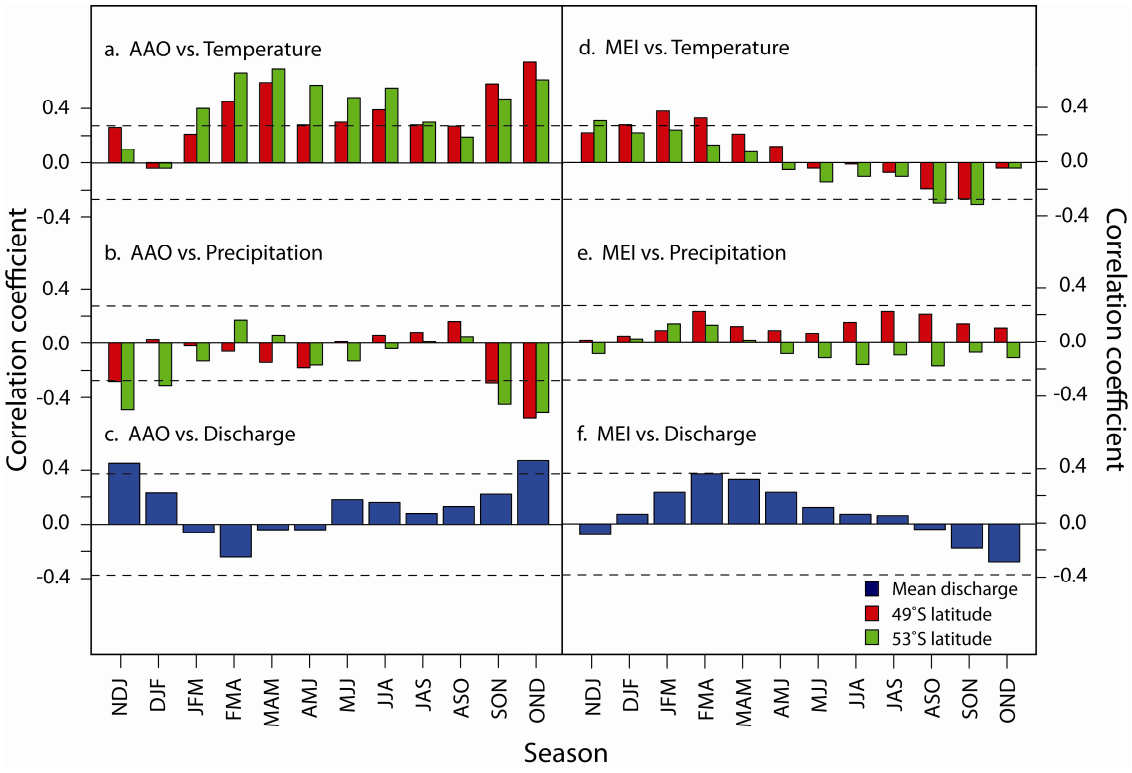

Figure 3.7. The Antarctic Oscillation correlated with temperature (a), precipitation (b) and discharge (c); the Mean ENSO Index correlated with temperature (d), precipitation (e) and discharge (f). Dashed horizontal lines indicate statistical significance at the 95% confidence level.

3.3. Tree-ring chronologies
3.3.1. Common signals and growth trends between site chronologies

Throughout the following sections, results from the tree ring sites will be discussed in two parts. The first part will address the chronologies developed in this study. The second part will focus on the regional chronologies, which incorporate sites developed in this study as well as additional sites contributed by other researchers.

The descriptive statistics for the three Heim sites and the three Torre sites are shown in Table 2.4 (Data and Methods). For all sites, the mean interseries correlation is above 0.54, indicating good agreement between the trees at a single site. Figure 3.8 shows the changes in the mean correlation among tree-ring series over the period of record. All chronologies except TN and HME exhibit persistent, relatively high correlations among series for most of the intervals. TN and HME both show a strong decrease in correlation between 1775 and 1800. Though less conspicuous, this dip is also present in TS, HME and TM4 (the HCO chronology does not extend far enough back in time to capture this period). The TM4 chronology has a second strong decrease in rbar between 1900 and 1925. Interestingly, TM4 has the highest mean correlation between trees (Table 2.4), indicating a strong common variance. HM4 shows the greatest variation in rbar, decreasing from an average greater than 0.3 before about 1875 to an average just over 0.2 in the 20th century. However, HM4 also has the lowest overall mean correlation (0.541), indicating a weaker common response to regional climatic forcing.

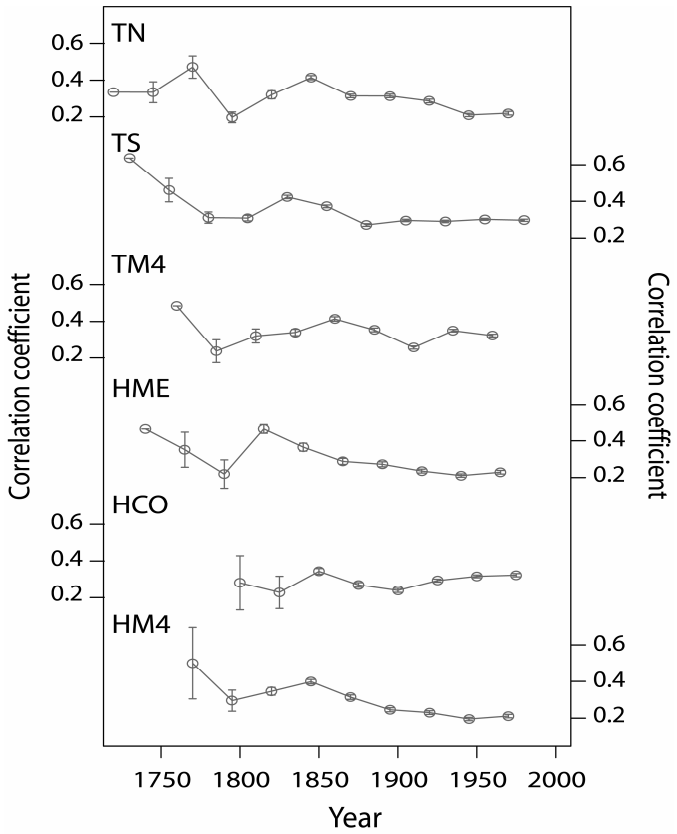

Figure 3.8. Mean tree-ring series correlation for the six chronologies developed for this study. Correlations are calculated using the Rbar output from the ARSTAN program. The moving window used for computing Rbar statistics is 50 years with a 25 year overlap between adjacent windows. The vertical bars represent the 2 standard error limits for the Rbar values. Site codes are given in Table 2.3.

All chronologies except HCO have EPS values over the threshold value of 0.85 (Wigley et al., 1986) after 1800. The HCO chronology only reaches this threshold level around 1830, likely due to low sample replication prior to 1815. The high EPS values after 1800 indicate temporal stability, good quality and a strong common signal for all the chronologies during the past two centuries.

Mean sensitivity (Fritts, 1976) and the standard deviation provide a more detailed understanding of the total variability in the chronologies. Although mean sensitivity does not vary greatly among the six sites, the Torre sites have a higher mean sensitivity than do the Heim sites. Similarly, the standard deviation of sites in Torre is typically slightly less than that of Heim sites. This suggests that sites in both valleys are equally stressed, although the higher mean sensitivity of the Torre sites may be attributable to the higher elevation of these sites.

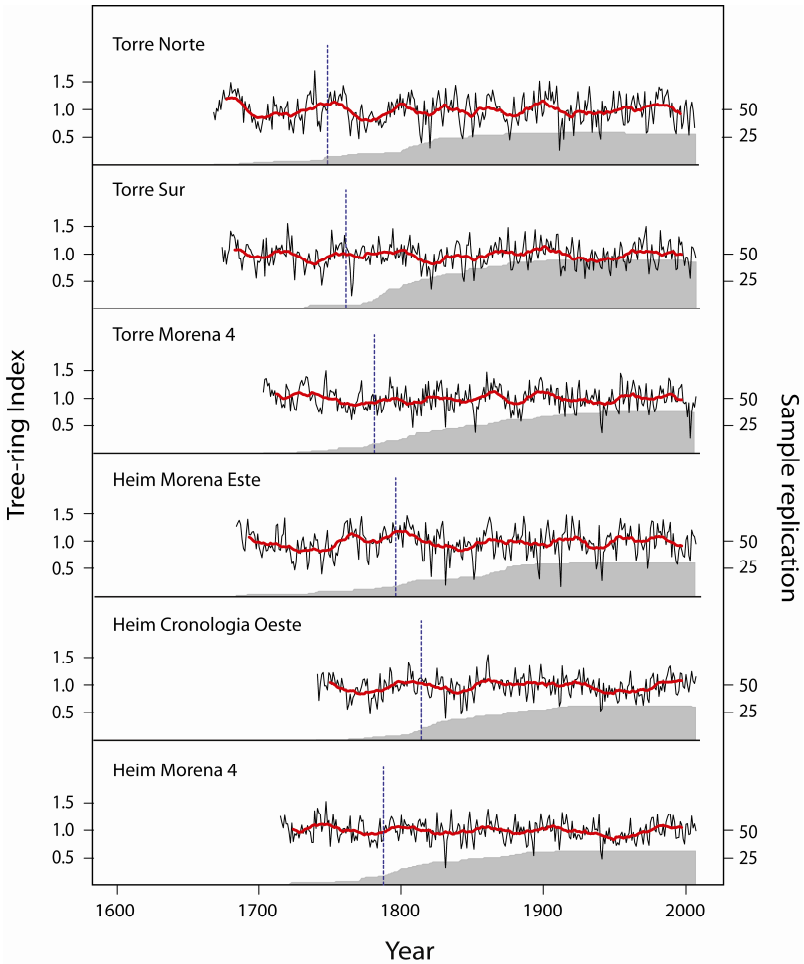

Figure 3.9. Tree ring indices for a 200-year spline detrending (black lines). The gray areas indicate the sample replication and the dashed lines indicate where sample replication falls below 10. The red line is the 10-year running mean.

Tree-ring growth patterns for the various chronologies show both inter-annual as well as low-frequency variations (Figure 3.9). The Torre chronologies show periods of roughly synchronous below-mean growth (1815-1830, 1880-1890, 1920-1950), whereas periods of above-mean growth are less coincident. The average interseries correlation among the three

Heim chronologies is 0.51. The average interseries correlation among the Torre sites is also 0.51 and when all six sites are combined, the correlation remains fairly strong at 0.45.

As discussed in section 2.4, the prevalence of fungal infection in *N. pumilio* prevented the collection of pith offset information for the majority of samples. In order to obtain a reasonable estimate of the difference in age trend and growth rates between sites, the series from all six sites were detrended *en masse* using RCS, re-divided into their respective site groups, and aligned by cambial age. Figure 3.10 shows the age-aligned chronologies (a) as well as the mean, RCS-detrended site chronologies (b). The cambial age graph suggests that the age trends at both Heim and Torre are predominately linear. As mentioned previously, trees at the Heim sites grow notably faster than those at the Torre sites, particularly Torre Sur (TS) and Torre Norte (TN). These two sites have very similar growth rates but differ considerably from Torre Morena 4 (TM4). This is can be explained by the difference in elevation between TS and TN, both situated near treeline, and TM4, which is located closer to the valley floor.

Without reliable pith offset information, the cambial age graph in Figure 3.10 can only provide a relative estimate of age trends and growth rates between the sites. To verify these assumptions, commonly detrended site chronologies can be plotted chronologically (Figure 3.10b). Although it is difficult to distinguish differences in age trend and growth rate between proximal sites with relatively low sample replications (~40), it is nevertheless clear that Torre sites have a generally slower growth rate than Heim sites. Tree growth at the Torre sites is particularly slower during the 19th century. Growth at Torre Sur remains low in comparison to the other sites throughout the 20th century, and growth at Heim East remains high. However, the distinction between growth rates within the two valleys becomes less evident in the 20th century. Growth rates at all sites except Torre Sur appear to accelerate in the 20th century, which could reflect the general warming trend observed in the individual temperature station records. However, these graphs must be interpreted with caution. Without reliable pith offset information, a range of living and dead material and further variance adjustment, this method can only be used to describe relative changes in age trends and growth rates.

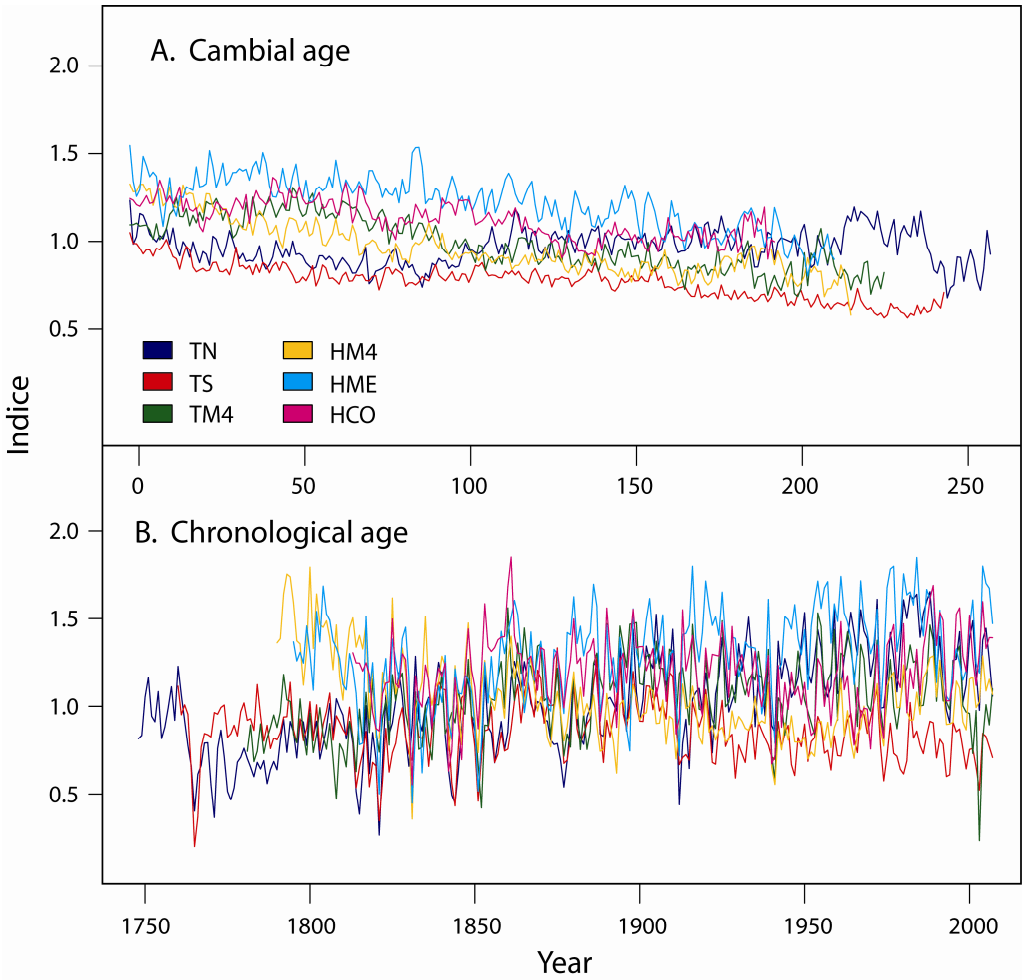

Figure 3.10. Site chronologies detrended in a single RCS run and plotted by cambial age (a) and chronological age (b). Both graphs indicate fairly linear age trends and slower relative growth rates at Torre sites than at Heim sites. Chronologies have been truncated where n < 10.

3.3.2. Common signals and growth trends between regional chronologies

As noted in section 2.3 (Data and Methods), the six chronologies discussed above and three additional chronologies were used to develop four regional chronologies with high sample replication and rbar (> 0.47). Torre Sur and Torre Norte were combined with a dataset from Glaciar Piedras Blancas to create the "Torre" chronology. Over their 325-year common interval (1694-1998), the three sites have a correlation higher than 0.60 ($p < 0.05$). Heim East and Heim Morena Four were similarly combined to develop the "Heim" regional chronology. The Heim sites correlate at 0.71 over their 266-year common interval (1741-2007; $p < 0.05$). Two additional regional datasets, PV1 and PV2 were contributed by Juan Carlos Aravena The *Pilgerodendron* datasets (PV1 and PV2) are from Chile provide 632-year long regional records for the western slope of the Andes at 49°S and 53°S. The four composite regional chronologies are shown in Figure 3.11.

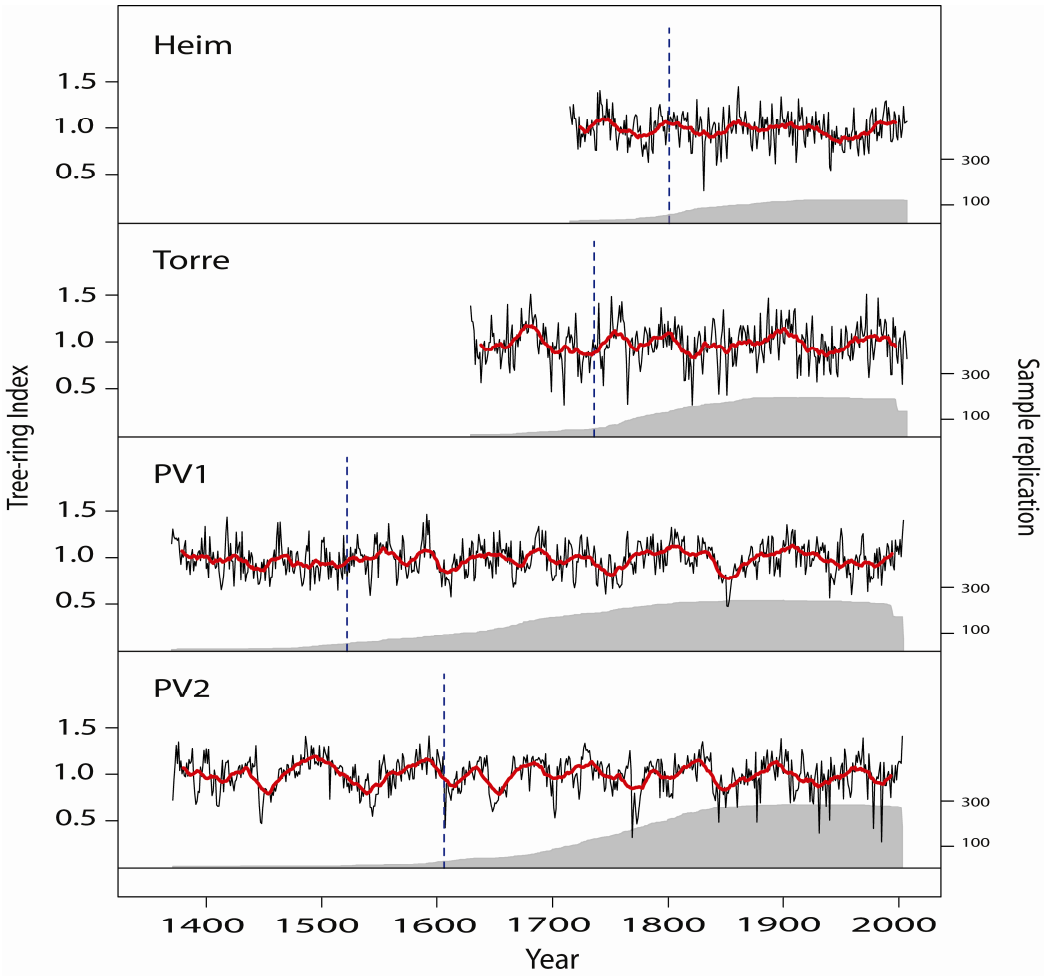

Figure 3.11. Regional composite chronologies detrended with a 200-year spline. Sample replication is shown in gray; the point at which sample replication drops below n=20 is indicated by the dashed vertical line; the ten-year running mean is shown in red.

Although only four regional chronologies were developed for this study, it is clear that correlation patterns of the regional chronologies show greater similarity between geographically proximal sites. The two regional *Nothofagus* chronologies (Heim and Torre) are significantly correlated ($p < 0.05$), and so are the *Pilgerodendron* chronologies. However, the *Nothofagus* chronologies do not correlate significantly with the *Pilgerodendron* chronologies. The mean correlation among tree-ring series for overlapping 50-year periods, or rbar, varies between 0.473 and 0.525 (Figure 3.12). All four chronologies have EPS values above the threshold value of 0.85 (Wigley et al., 1986) after 1810. This indicates temporal stability, good quality and a strong common signal for all the chronologies during the past 200 years. EPS for the two longer *Pilgerodendron* series is strong after 1605 and the EPS for the Torre chronology is above 0.85 from 1680. As the EPS threshold of 0.85 corresponds to a sample size of 20 or higher, chronologies were truncated where $n < 20$ rather than at $EPS > 0.85$ for simplicity.

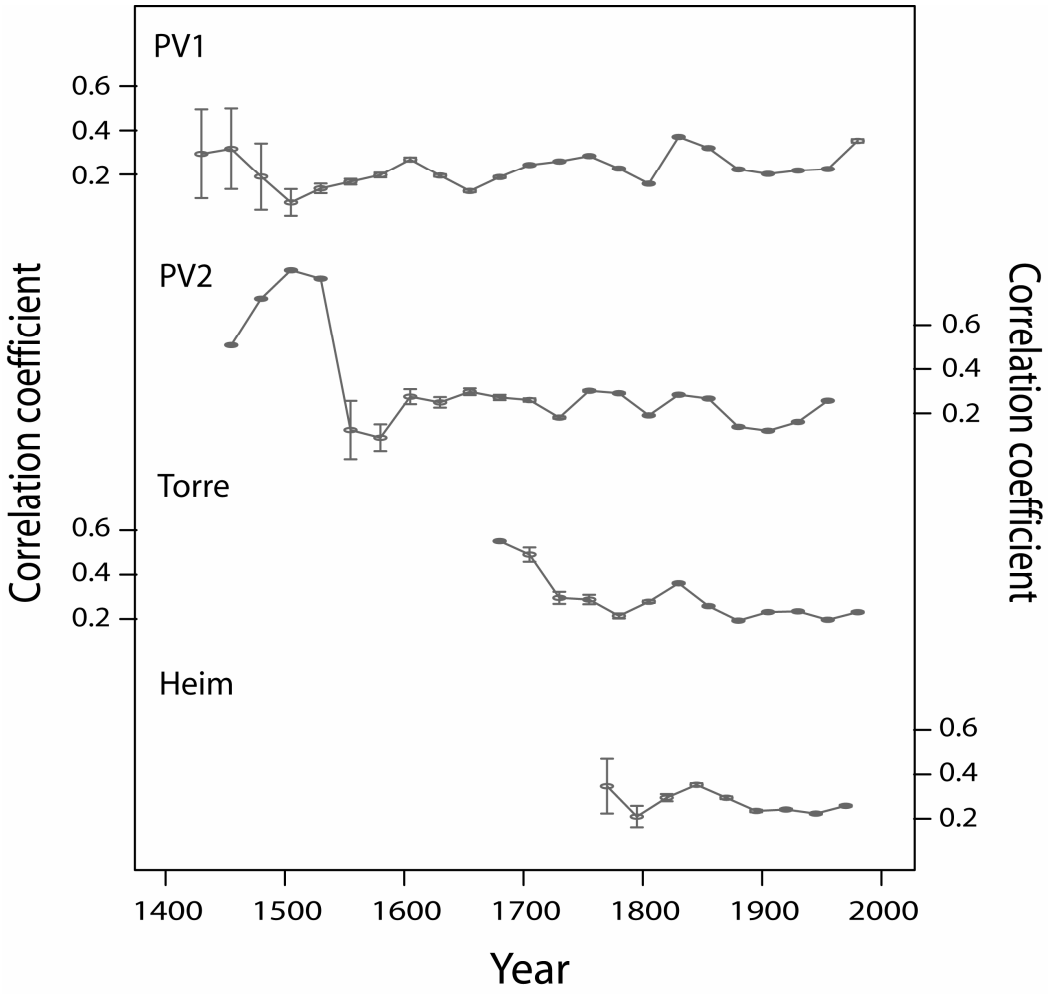

Figure 3.12. Mean tree-ring series correlations for the four regional chronologies developed for this study. Correlations are calculated using the Rbar output from the ARSTAN program. The moving window used for computing Rbar statistics is 50 years with a 10 year overlap between adjacent windows. The vertical bars represent the 2 standard error limits for the Rbar values. Site codes are given in Table 2.3.

Lara *et al*. (2005) used a similar method for grouping tree-ring chronologies to describe *Nothofagus* growth at tree line. They developed a total of thirteen regional composite chronologies for the Chilean Andes between 35°40'-55°S and obtained results very similar to those found in this study. In general, the composite chronologies developed in this study have higher rbar values and higher mean sensitivity but larger standard deviation and autocorrelation. These differences may stem from the fact that Lara's chronologies span a wider latitudinal range.

As noted in the previous section, reliable pith-offset data are not available for the chronologies. In order to obtain a reasonable estimate of the growth trends for each regional chronology, all sites were combined and detrended in a single Regional Curve Standardization (RCS) run. Figure 3.13 shows the resulting time series, plotted by cambial age and by chronological age. Although the caveats described in 3.2.1 regarding the accuracy of the estimations of age trend and growth rate remain valid, the graphs in Figure 3.13 allow for a relative understanding of regional differences in growth rates and trends. The Torre, Heim and PV2 composite chronologies exhibit a fairly linear age trend in which growth is rapid during the early decades of the tree's life and slows with increasing age (Figure 3.13a). The growth trends of the *Pilgerodendron* composites are flatter than those of

the two *Nothofagus* composites, probably due to the difference in species longevity. The PV1 chronology, however, exhibits a sudden decrease in growth rate when trees reach 100 to 150 years of age. After about 200 years, the growth trend resembles that of PV1.

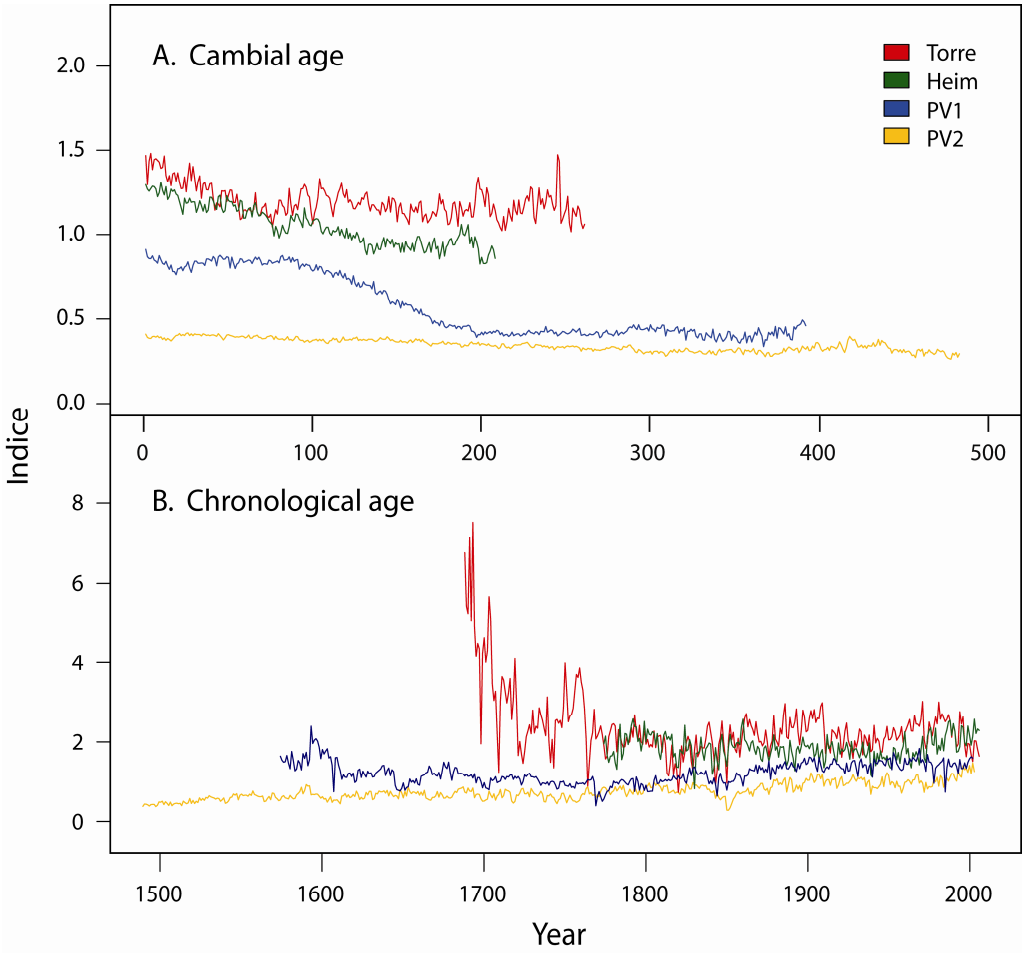

Figure 3.13. Regional chronologies detrended in a single RCS run and plotted by cambial age (a) and chronological age (b). Chronologies are truncated where sample replication falls below 20.

When plotted by chronological age (Figure 3.13b), the Torre chronology appears to enjoy the most favorable growth conditions and the greatest variability, whereas the PV1 chronology has the slowest growth rate and relatively little variability. Although PV1 and PV2 are the only chronologies long enough for such an observation to be made, it appears that there is a slight increase in the growth rate and variability from 1800 to present and particularly since approximately 1950. Further analysis is needed to verify this trend, but an increase in growth rate over the last two centuries would correspond to the increasing temperatures observed in southern South America (see Sections 3.1.1 and 3.1.4).

3.4. Growth-climate relationships

The strength of the correlations between the four detrended (200-year spline) composite regional chronologies and the instrumental records indicate the relative importance of temperature and precipitation as environmental controls of *N. pumilio* radial growth at each site. As most samples were collected near tree line, it was expected that temperature would be the most important factor for tree growth. However, tree-ring indices were also compared with discharge records, as the temperature-discharge relationship in the Santa Cruz basin indirectly indicates soil moisture. Higher temperatures trigger an increase in meltwater runoff throughout the upper basin, water that is potentially available for tree growth.

3.4.1. Precipitation correlations

Precipitation plays a minor role in the radial growth of *N. pumilio* and appears to have a delayed influence on the growth of two *Pilgerodendron* chronologies (Figure 3.14). Precipitation at 49°S is generally negatively correlated with tree growth at Heim and Torre throughout the year, possibly because precipitation falling as snow limits the growing season. However, the samples for these sites were collected with the expectation that temperature, not precipitation, would be the main factor controlling tree growth. The *Pilgerodendron* chronologies are also expected to be more temperature-sensitive. As the trees from these sites are located on the more humid western slope of the Andes, however, precipitation is expected to have more influence on tree growth. Indeed, tree growth at both PV1 and PV2 responds positively to precipitation, particularly during the growing season. PV1 in particular correlates significantly ($p < 0.05$) with precipitation between November and February.

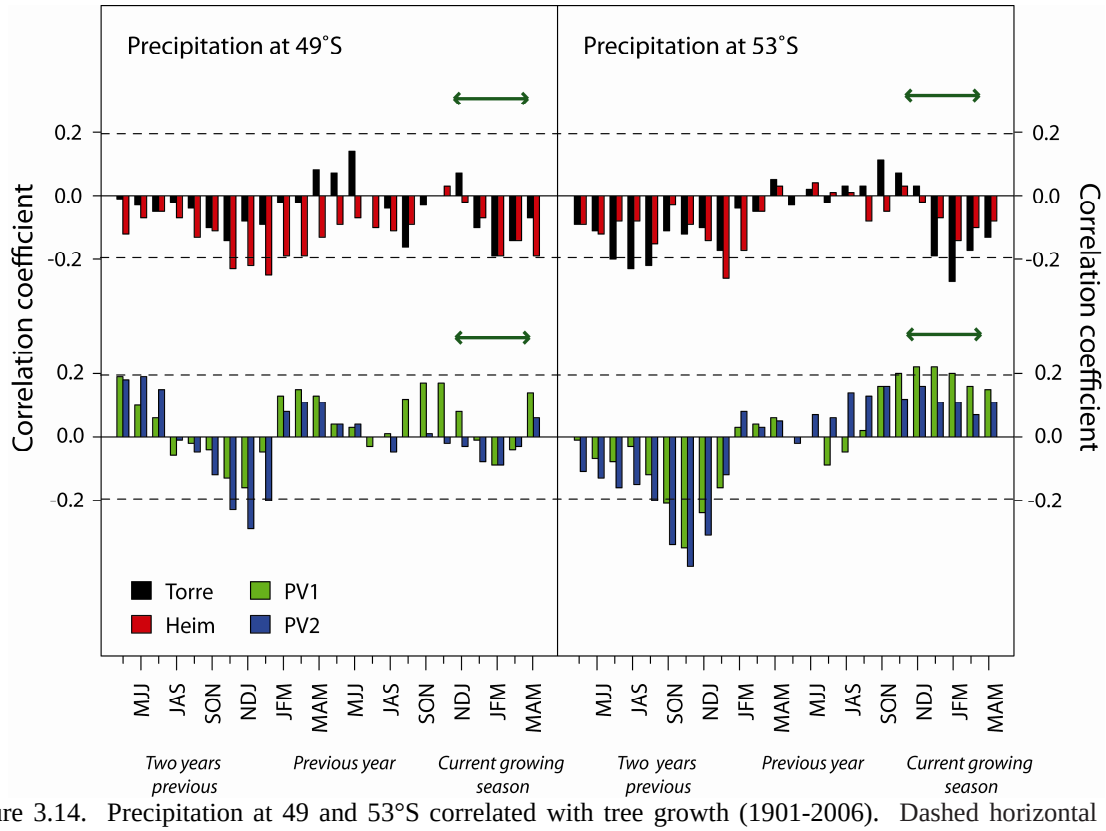

Figure 3.14. Precipitation at 49 and 53°S correlated with tree growth (1901-2006). Dashed horizontal lines indicate statistical significance at the 95% confidence level; the green arrows indicate the growing season.

Interestingly, the strongest correlations occur between tree growth and precipitation occurring two years prior to the current growing season. The correlation is strongly negative ($p < 0.05$). This may be interpreted as a memory effect, indicating that *Pilgerodendron* is sensitive to the soil moisture reservoir or to moisture stored in the snow pack. It may also be considered as a data artifact, but it is interesting to note that tree growth at Heim and at Torre is also rather strongly negatively correlated with precipitation occurring two winters before the current growing season. Aravena et al. (2002) observed a similar relationship between radial growth and precipitation in southern Chilean Patagonia. They concluded that the negative correlation indicates that tree growth may be negatively affected by an extended snowfall season associated with higher precipitation years. Such a relationship has also been described for Northern Patagonia in Argentina at 41°S (Villalba et al., 1997).

With the exception of PV1, it may be concluded that precipitation does not play a significant role in the radial growth of the composite chronologies. However, as noted in Section 3.1.4, the majority of precipitation falling in the study area occurs during the fall and winter months, when growth has stopped. While the amount of precipitation that falls in the months proceeding growth may be an important factor in determining soil water availability during the growing season, this relationship cannot be adequately captured by a simple growth-precipitation correlation relationship.

3.4.2. Temperature correlations

In contrast to expectations during sampling, the relationship between temperature and radial growth is not especially strong (Figure 3.15). However, unlike correlations between tree-growth and precipitation, the correlation patterns for temperature are very similar for all four sites. Growth at all sites is positively correlated with temperature during the fall and winter months of the preceding year (May to September) and negatively correlated with temperatures during the spring and summer (October to March). The reasons for this relationship are not clear. Previous studies of tree-growth of *N. pumilio* forests at the upper treeline in the southern Chilean Patagonia (Aravena et al., 2002), in the Argentinean Tierra del Fuego and Isla de los Estados (Boninsegna et al., 1989) and in northern Patagonia at 41°S (Villalba et al., 1997) have all found a positive correlation with temperature.

Much further north, between 35° 36’S and 37° 30’S, radial growth has been shown to be negatively correlated with late-spring and early-summer temperature (Lara et al., 2001). This relationship also seems to be true of the *Pilgerodendron* sites used in this study despite their much more southerly location. A possible explanation for this relationship is that higher summer temperatures result in increased evapotranspiration, while warmer conditions during the fall allow for a longer period of growth once the rainy season begins.

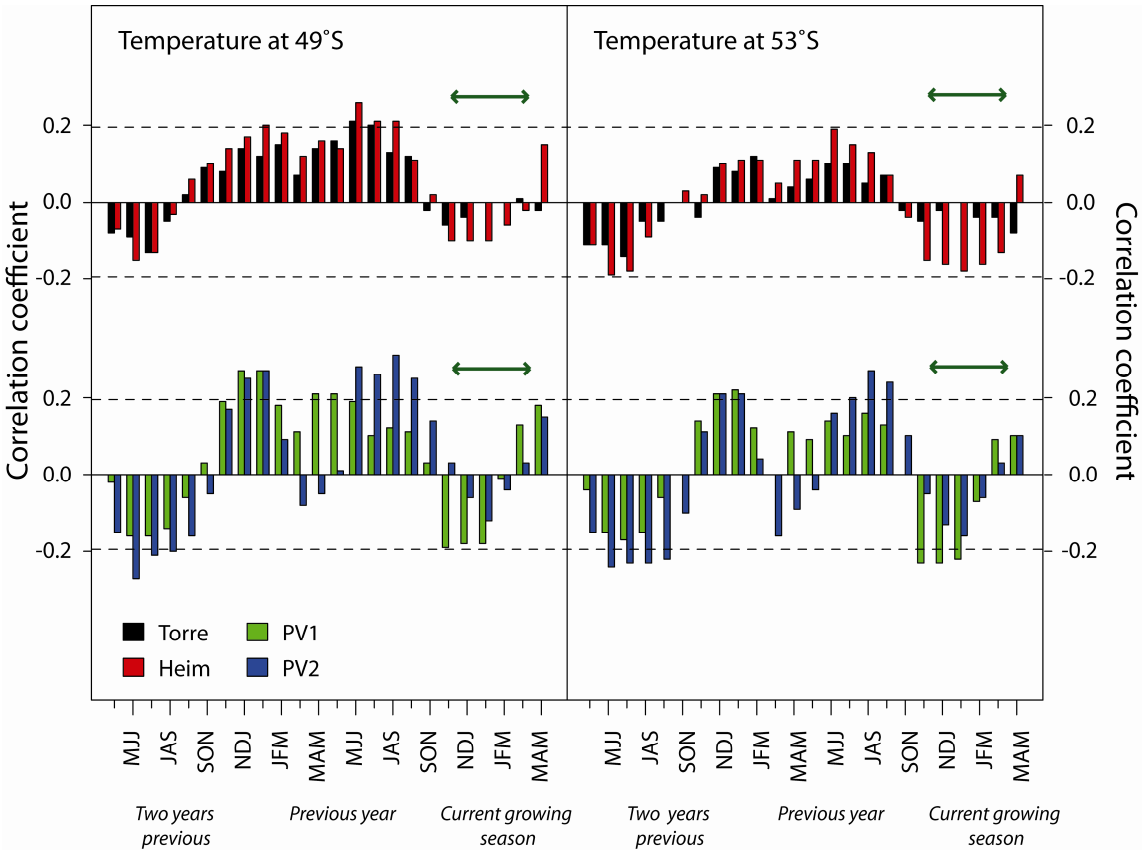

Figure 3.15. Temperature at 49 and 53°S correlated with tree growth (1901-2006). Dashed horizontal lines indicate statistical significance at the 95% confidence level; the green arrows indicate the growing season.

3.4.3. Discharge correlations

Like temperature, the relationship between tree growth and discharge is not especially robust (Figure 3.16). In spring (SON), the correlation between discharge and radial growth at Heim is significant ($p < 0.05$) though not strongly. The correlation strength remains fairly stable through the early summer (NDJ). In section 3.2, it was noted that temperature and discharge are strongly correlated in the spring and summer. Bearing this in mind, the positive discharge-growth relationship in the spring can be interpreted as being strongly dependent on temperature. Rising temperatures in the spring prompt the release of moisture held in the snow pack and thaw the ground. Water therefore becomes available for use by the trees. Discharge may in this case be a proxy for soil moisture, which may play a more direct role in tree growth than temperature or precipitation alone.

The relationship between discharge and growth at Torre, PV1 and PV2 is not so easily explained. For these sites, the peak correlation occurs several months earlier, in mid- to late winter. Although some variation in the response to discharge (or temperature) is expected, it is interesting that the northernmost (Torre) and southernmost (PV2) sites should respond at the same time. It is also interesting that Torre and Heim, which are relatively close to one another, should show such distinct responses to discharge. However, the early response to discharge corresponds with the positive temperature-growth correlations observed in Figure 3.15. There is also a consistent positive correlation between tree growth at PV2 and discharge occurring two years prior to the current growing season that is not mirrored in the temperature-growth correlations. At PV2, this relationship is almost significant (0.05). Both

PV1 and Torre show a similar positive correlation. The reason for such a relationship is not clear but may be due to a memory effect within the trees.

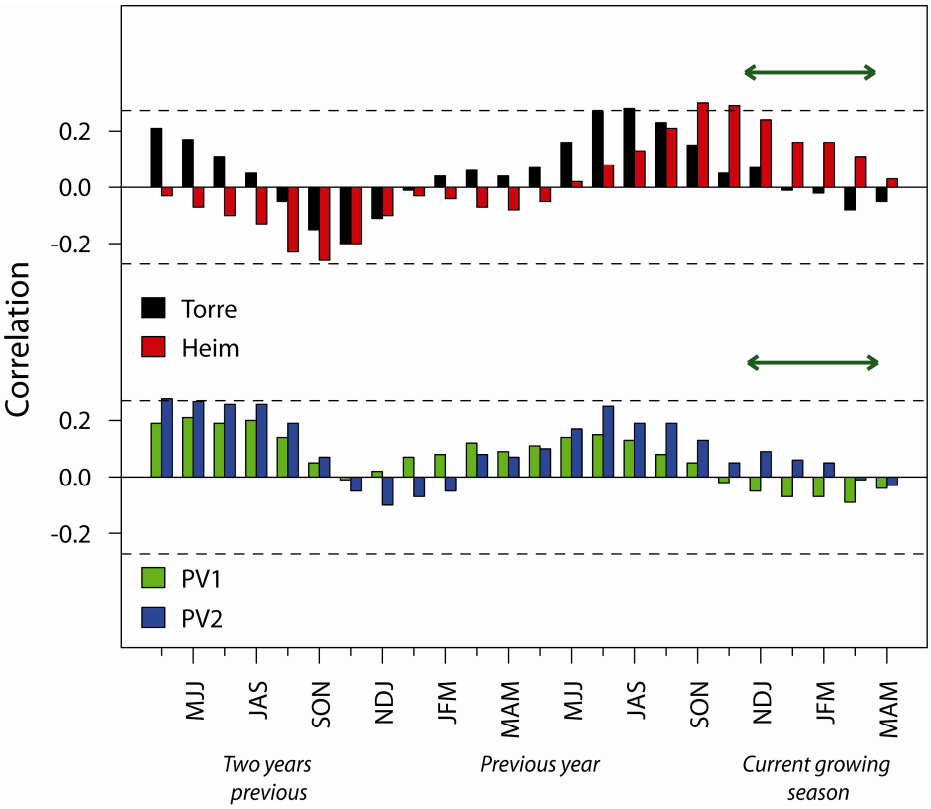

Figure 3.16. Correlations between tree growth and the mean discharge record (1956-2006). Dashed horizontal lines indicate statistical significance at the 95% confidence level; the green arrows indicate the growing season.

One of only two streamflow records developed for Patagonia to date is the recent reconstruction by Lara et al. (2008). A strong positive correlation between tree-ring width and previous summer and fall Puelo River streamflow ($p < 0.05$) was found in this study. The reconstruction is focused on a more northerly location (~41.5°S) west of the Andes and utilizes different trees species (*Austrocedrus chilensis* and *Pilgerodendron uviferum*), but it is interesting that there is a notably different seasonal response to discharge. A second streamflow reconstruction exists for northern Patagonia and focuses on the eastern slope of the Andes (Holmes, 1979). Holmes does not specify any seasonal discharge-growth relationships but was able to reconstruct streamflow on the Neuquén and Limay rivers with a high degree of correlation between the reconstructed and gauged records. Further work is clearly needed in the Patagonian region before the relationship between streamflow and tree growth can be fully understood.

3.4.4. AAO/MEI correlations

Distinct temporal patterns emerge when the temperature, precipitation and discharge data are correlated with the radial growth records. However, these relationships are neither particularly strong nor spatially distinct. Two large-scale climate patterns affect the climate of southern South America, the Antarctic Oscillation and the El Niño/Southern Oscillation (recorded in the MEI). To test whether either of these patterns noticeably influences radial growth, AAO and MEI indices were compared to the ring-width chronologies.

The relationship between the AAO and tree growth shows a clear seasonal pattern but is almost entirely non-significant. The northernmost *Pilgerodendron* chronology, PV1, is the only exception and is significantly but not strongly positively correlated with the AAO in early winter (MJJ) preceding growth ($p < 0.05$). The other three chronologies do not exhibit a notable positive correlation with AAO during the winter months and in fact the Heim and Torre sites are slightly negatively correlated with the AAO over this period. These three sites instead have a positive but still non-significant correlation with the AAO in the spring and early summer (OND-NDJ). PV1 is negatively with the AAO during these months.

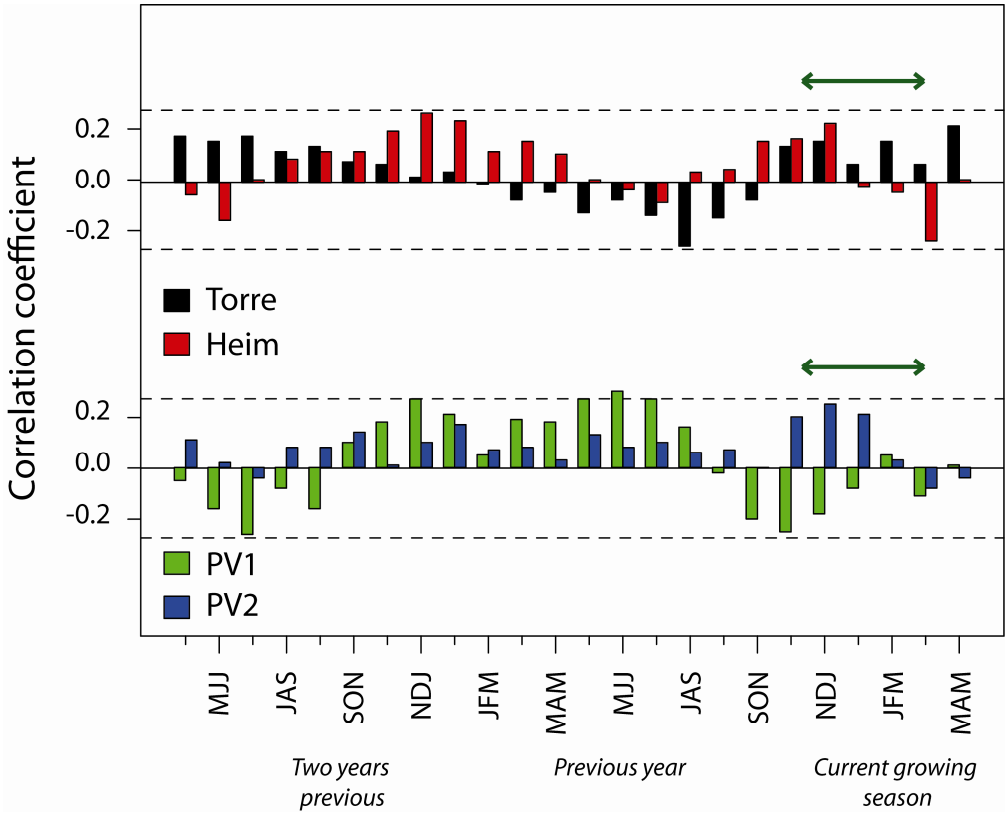

Figure 3.17. Correlations between the AAO and tree growth (1979-2006). Dashed horizontal lines indicate statistical significance at the 95% confidence level; the green arrows indicate the growing season.

The reason for such disparate responses to the AAO is not apparent. As noted in section 3.2, neither the climatic nor the hydrologic records show any strong seasonal correlation with the AAO during the winter months. Instead, positive values of the AAO correspond to increased temperatures and discharge in the spring and early summer. Warmer temperatures and increased water availability at the beginning of the growth season may explain why Torre, Heim and PV2 show a positive correlation with AAO in the spring.

Thompson and Solomon have found that the positive phase of the AAO is associated with cooling over most of Antarctica, with the exception of the Antarctic Peninsula and southern South America (2002). In these regions, the anomalously strong westerlies related to the high AAO polarity prevent the incursion of cold air from the south and increase the advection of relatively warm oceanic air over the land. Annual temperature variations in southern Patagonia, reconstructed from a network of upper-treeline *N. pumilio* chronologies (Villalba

et al., 2003), have been shown to be significantly correlated with annual variations in the AAO index.

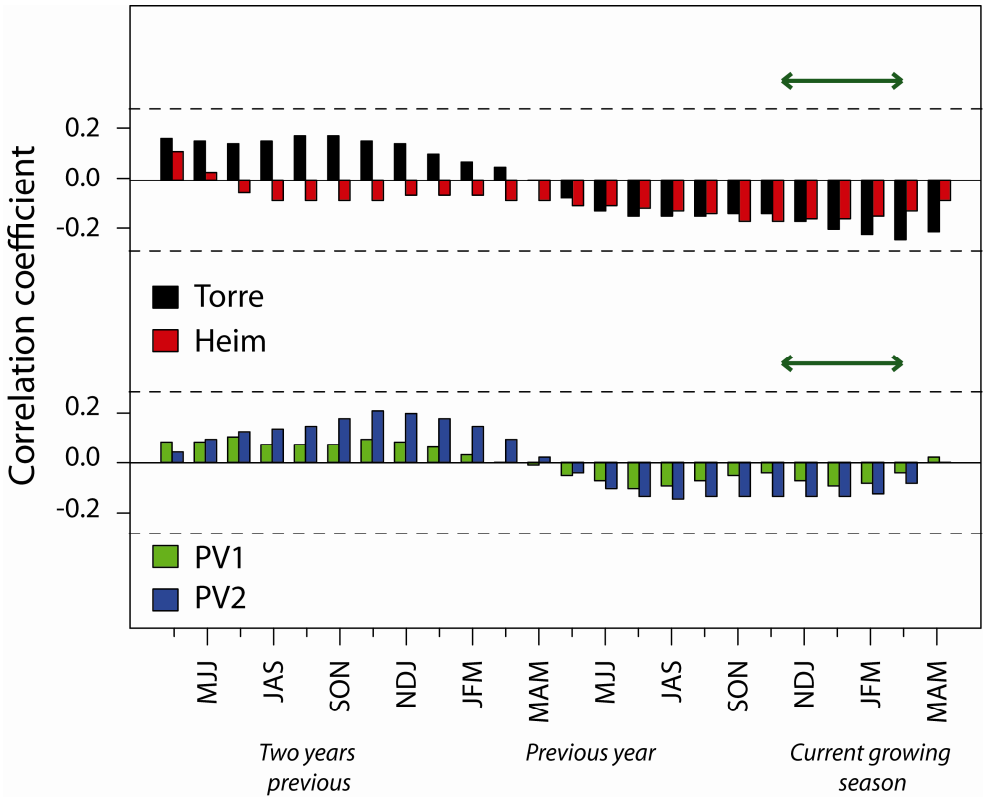

Figure 3.18. Correlations between the MEI and tree growth (1950-2006). Dashed horizontal lines indicate statistical significance at the 95% confidence level; the green arrows indicate the growing season.

The relationship between MEI and radial growth was also examined on a seasonal basis. ENSO is known to significantly influence interannual to decadal climatic variability (Daniels and Veblen, 2000) and has been shown to influence important ecological processes in northern Patagonia (Villalba and Veblen, 1997, 1998; Villalba et al., 1998).

As Figure 3.18 illustrates, a strong oscillatory pattern exists for all chronologies but does not reach significant strength. From the fall (MAM) of the preceding year to the fall of the current year, radial growth is negatively correlated with the MEI. Thereafter, the correlations with MEI become positive. The strongest correlations, particularly at Torre, occur during the spring and summer of the current growing season. This period encompasses the peak ENSO season (November-February), when warm and cold events typically mature in the equatorial Pacific (Christie et al., 2009).

Without further analysis, the significance of these correlations is difficult to interpret. Other studies of tree growth in relation to ENSO have yielded results that are highly dependent on latitude and whether the trees grow on the eastern or western slope of the Andes. In the tropical central Andes, two high-elevation *Polylepis tarapacana* chronologies were developed along the Western Cordillera to determine the ENSO signal strength present in the tree-ring records (Christie et al., 2009). The authors found a significant correlation with spring-summer (August-February) SST in the Niño3.4 region and noted that the chronologies show oscillatory modes within the classical ENSO bandwidth. Further south, at approximately 41°S, *Austrocedrus chilensis* was used to develop a 400-year long

precipitation reconstruction for northeastern Patagonia (Villalba et al., 1998). The reconstruction exhibited significant oscillations within the preferred frequency domain of ENSO, but no clear and consistent responses to ENSO were observed. At the same latitude, samples from high-altitude *Nothofagus* forests on both sides of the Andes were used to study the spatiotemporal influences of climate on altitudinal treeline (Daniels and Veblen, 2004). The authors found that ENSO significantly influenced tree growth west of the Andes, but that correlations with the ENSO indices were weak or inconsistent between sites east of the Andes. Given the varying results of these three studies, further investigation is needed before the results of this study can be properly interpreted.

Chapter 4 - Conclusions

4.1. Summary

The rapid retreat of South American glaciers has been well-documented over the past four decades (Kaser and Georges, 1990; Naruse et al., 1997; Aniya et al., 1996, 1997, 1999; Rignot et al., 2003; Rasmussen et al., 2007; see references in Carey, 2005). Glaciers in the tropical Andes have been shown to be particularly sensitive to the increasing temperature trend observed throughout much of South America (Rösenbluth et al., 1995, Rösenbluth et al., 1997, Jones et al., 1986) and many glaciers are expected to disappear completely within the next fifty years (Mark and Seltzer, 2003, 2005; Francou et al., 2003). Particularly in western South America, the Andean glaciers serve as vital reservoirs of fresh water and are especially important for ensuring water supply during the dry season. Human activities, namely hydropower production and agriculture, are reliant on the long-term supply of glacial runoff. The hydroelectric system along the main, glacier-fed rivers in semi-arid Patagonia, for example, produces more than 25% of the total energy consumed in Argentina (Quintela et al., 1996). Without the glacier-supplied river water, the people and economies of the region would have to undergo tremendous adjustments.

Sound management of a limited and changing water supply depends on a thorough understanding of the climate-glacier-streamflow relationship. The physics governing the Andean glaciers – and hence streamflow – are more complicated than simple temperature forcing (Barnett et al., 2007). Predictions of what might happen in the Andes are therefore difficult and depend on latitude and which side of the Andes is considered. Predictions are further complicated by the relatively short temporal and sparse spatial coverage of meteorological records, which seldom exceed seventy years and have a density of approximately 40,000 km^2 per station (Paruelo et al., 1998). As a result, the instrumental record will only manifest a small amount of the inherent variability and only at limited frequencies. Furthermore, it is unlikely that the climate recorded during the past half century is representative of that of previous centuries (Bradley and Jones, 1992).

The extension of climatic and hydrological records in southern Patagonia – on *both* sides of the Andes – should improve our understanding of the hydroclimatic variability in this region. Tree-rings provide one means of estimating the decadal to century-scale oscillatory modes in climate variability over the last few millennia by providing long, well-replicated series with annual resolution (Villalba et al., 1998). In a region influenced by an array of complex factors, including strong zonal windflow, significant topographic barriers, a vast icefield and strong climatic gradients over relatively short distances, tree rings also provide unrivaled spatial information. The development of multiple tree-ring chronologies throughout southern South America helps to disentangle the role these factors have played in Patagonian climate over the last several centuries.

In the introduction, four key questions were presented. The following sections present the conclusions reached during this thesis work regarding each of these sections and suggest for future lines of investigation.

4.2. How can we best deal with the limited instrumental climatic and hydrological records available to us?

The availability and reliability of instrumental data is one of the greatest challenges to overcome when working in southern South America. As noted above, few meteorological stations are available in southern Patagonia and much of the data that is available covers a limited timespan and contains significant gaps. The seven meteorological stations used in this study are the only official meteorological stations available between 48°S and 53°S. Similarly, the five hydrological stations represent a watershed that covers nearly 30,000 km^2. Three of these records provide less than eleven years of data.

Despite these challenges, the instrumental data provide snapshot understandings of the geographical differences in Patagonian climate. Perhaps the most pronounced difference is the west to east climate gradient resulting from the orographic blocking action of the Andes. Meteorological stations on the windward side of the Andes annually receive over thirty times more precipitation and generally exhibit less temperature variability than their eastern counterparts. Stations on the eastern side of the Andes describe a much drier climate with a greater annual temperature range. Indeed, west to east differences in temperature and precipitation are mirrored in the west to east differences in climate trends over the past half century. Stations east of the Andes generally exhibit stronger increasing temperature trends than western stations. Similarly, the western precipitation records exhibit a decided decrease in precipitation over the last half century. Both trends have been recognized in previous studies (Rösenbluth et al., 1995, 1997; Rivera et al., 2000, 2002, 2005; Villalba et al., 2003, 2005; Rivera, 2004; Masiokas et al., 2008).

To avoid the complications inherent in using climate time series that cover different time periods with varying continuity, gridded climate data was used for comparison with the tree-ring and hydrological records. Gridded 2.5 x 3.75 degree precipitation and temperature data for cells centered between 49°S and 50°S and between 53°S and 54°S were obtained from the Climate Research Unit. These datasets offer homogenized, universally available climate information for the past one hundred years and represent data from the individual stations reasonably well. A "mean" hydrological record was similarly obtained by combining the standardized anomalies of the two longest records (Charles Fuhr and La Leona).

While the use of these records simplifies the analysis process, the resulting comparisons with other instrumental records and with the tree-ring series suggest that CRU data resolution is too coarse to fully capture the range of climatic variability occurring in this topographically diverse region. For example, the relationships between temperature and discharge and precipitation and discharge are not as strong as might be expected in a hydrological system that is almost entirely dominated by melt water. A more localized temperature record, for example, would likely show a stronger relationship to discharge than the gridded data, which were derived from temperature records over a broad region. This conclusion is particularly relevant for precipitation, a factor with high inherent spatial variability.

However, the CRU data do reveal some obvious climatic differences between sites located at 53°S and those at 49°S. At the more southern location, temperature and precipitation tend to oscillate together. Most precipitation occurs during the late summer at 53°S, whereas the dry season corresponds to the winter months (June-August). In contrast, peak precipitation at 49°S occurs when temperatures are lowest, during the winter months. As a result, trees

growing at the upper treeline at 49°S reflect a mixed temperature-precipitation signal whereas trees at 53°S exhibit a more pronounced temperature signal.

Like the climate-discharge relationships, climate-growth relationships are not as strong as expected. The reasons for this are two-fold. First, the use of CRU data means that tree-growth is compared to a regionally averaged climate signal. Particularly strong departures from the mean climatology are therefore underemphasized. Second, southeastern Patagonia is a very harsh region, with low annual mean temperatures, limited precipitation and strong winds. Although the cold- and dry-treelines are visually distinct, it is unlikely that either factor is strongly dominant at its respective treeline. Furthermore, the altitudinal difference between the two treeline types is not particularly great, varying between approximately 250 and 500 meters in some places. Similar mixed growth responses have been noted in other cold-dry environments such as Maritime French Alps (Büntgen et al., in press), western Iberia (Gea-Izquierdo et al., 2009) and the Eastern Alps (Di Fillippo et al., 2007).

The strength of the interseries correlations among the tree-ring series, both the individual sites and the composite regional chronologies, indicates that trees are responding to a common signal. Defining the exact nature of that signal, however, is complicated. As noted above, complications arise from using climatic data that is perhaps overly generalized and by the complex array of factors influencing tree growth in southern Patagonia. More site-specific meteorological records could potentially be developed by combining only records from meteorological stations close to the sampling sites, similar to the mean hydrological record developed in this study for the Río Santa Cruz. These records would not provide the temporal coverage that the gridded data sets do, but they would be more representative of the climatology at the sampling sites.

However, official meteorological stations in southeastern Patagonia are generally located far from the actual tree-ring sites, typically at lower elevations and in warmer and drier regions (e.g., El Calafate). Short-term climate data (< 10 years) exist for specific regions much closer to the tree-ring sites (i.e., Srur et al., 2008). Regressions between these time series and longer ones available from official meteorological stations may allow for the comparison of tree-ring chronologies with adjusted, longer-term meteorological records.

A third alternative would be to use a different gridded dataset (e.g., University of Delaware, National Climate Data Center GHCN and others). Although the basic climate data used to construct the gridded datasets comes from the same station observations, the data is homogenized, weighted and compiled using different methods and spatial resolution.

4.3. How are streamflow and tree growth related to atmospheric circulation?

Relationships between large-scale atmospheric patterns, streamflow and tree-growth in southern Patagonia were evaluated in this study. Two climate indices were used, the Antarctic Oscillation (AAO) and the Mean ENSO Index (MEI). AAO and ENSO represent the two dominant modes of climate variability in southern South America and were expected to have a significant influence on climate and tree growth in the study area. Indeed, significant relationships were observed between AAO and temperature (positive correlations) throughout most of the year and between AAO and precipitation (negative correlations) and discharge (positive correlations) during the spring and early summer. The MEI exhibited a weaker seasonal correlation with these variables, but was significantly positively correlated with summer temperatures and discharge (which lagged temperature by about one month).

Thus, the positive phase of the AAO is linked to warmer winter and spring temperatures, which drive an increase in discharge. Similarly, the summers following El Niño episodes tend to be relatively warm and dry (Villalba et al., 2007), conditions that result in an increase in meltwater runoff with a typical one-month lag. If precipitation records of sufficient length can be obtained for the South Patagonian Icefield, it would be informative to compare such data with the discharge records in southeastern Patagonia. The majority of the discharge volume of these rivers is meltwater derived from the icefield. The icefield itself is cradled between the Andean peaks and receives the bulk of the precipitation carried by the westerlies, which are strongly influenced by ENSO and AAO. An analysis of precipitation over the icefield and discharge east of the Andes would provide a deeper understanding of the influence these large-scale climate patterns have on discharge in southeastern Patagonia.

Like the CRU data, the mean hydrological record is perhaps an oversimplification of the hydrological processes occurring in the Santa Cruz basin. The two time series used to construct the record are taken from stations located at the far ends of two very large lakes that undoubtedly dampen the runoff signal. Unfortunately, long, dependable records of discharge closer to the Andes do not exist. The mean hydrological record represents a reasonable means of overcoming the data inadequacies but conclusions about its relationship to climate and tree-ring data should be made with caution.

Although correlations between tree growth and the two climate indices show distinct temporal relationships, neither the AAO nor the MEI significantly influences tree growth in any of the four regional chronologies. In general, tree growth is positively correlated with the AAO in the spring. This relationship is likely due to the advection of warm oceanic air over southern Patagonia during the positive phase of the AAO. This warm - and potentially moist – air occurring early in the growth season promotes a positive growth response in the trees. Correlations between MEI and radial growth are less strong but exhibit a strong oscillatory pattern at all sites. The strongest correlations occur during the peak ENSO season (spring and summer), indicating that the trees are sensitive to ENSO but that the nature of this relationship is not fully captured in this study.

This study only looks at the relationship between the MEI and tree-growth but several other records of ENSO variability, such as the Southern Oscillation Index and sea surface temperatures, exist. These records may provide a more concise understanding of the relationship between ENSO and tree growth in southeastern Patagonia. It would also be interesting to compare years of maximum and minimum tree growth with instrumental (Trenberth, 1997) or reconstructed (Cook et al., 2008) records of El Niño and La Niña events.

Given the complex array of factors influencing tree growth, further investigations should also include analysis methods that would help to clarify non-linear relationships between tree growth, climate and atmospheric circulation. Composite analysis could, for example, be used to determine if years of minimum or maximum tree growth correspond to specific phases of ENSO or AAO. Similarly, spectral analysis would help to identify cyclical patterns in tree-ring, instrumental and climate indices data.

4.4. What is the role of the South Patagonian Icefield in modulating discharge?

The South Patagonian Icefield plays a major role in modulating the discharge of the Río Santa Cruz and other rivers of southeastern Patagonia. At El Calafate, the station nearest the Andes and the study sites, mean annual precipitation is less than 150 mm, a number that decreases with increasing distance from the Andes. Furthermore, the majority of precipitation falls as snow during the winter months. The Río Santa Cruz is therefore almost entirely dependent on snow and glacial meltwater, which are in turn dependent on temperature. As temperatures rise in the spring, runoff from melting snowfall and glacier ice swells the Río Santa Cruz. Peak discharge occurs about a month behind peak temperature, which indicates both a temperature-dependent meltwater response and the distance the runoff volume must travel before it is recorded by the gauging station.

The exact nature of the relationship between the South Patagonian Icefield and discharge can only be partially inferred, namely with temperature. However, the amount and timing of precipitation falling over the icefield and how these factors affect discharge east of the Andes is virtually unknown. As noted above, precipitation records from the icefield itself would shed considerable light on this relationship. However, monthly variations in ice mass as recorded by the Gravity Recovery and Climate Experiment (Chen et al., 2007) may also prove helpful in quantifying the icefield-discharge relationship.

4.5. Can we develop a reliable reconstruction of Río Santa Cruz streamflow for the past 2-3 centuries?

Given the dependence of human activities on the long-term health of glaciers and rivers in southern Patagonia and a corresponding lack of hydrological and climatic information, further research is needed to evaluate the full range of natural hydroclimatic variability in the Santa Cruz basin. The various challenges that must be overcome before a hydroclimatic or streamflow reconstruction can be developed for the Río Santa Cruz have been reviewed at length in this study. Trees on both sides of the Andes clearly respond to similar climatic signals but the exact nature of that signal is complicated by harsh climatic conditions, complex topography and limited instrumental records.

Suggestions toward overcoming these challenges have been presented and include the incorporation of ice mass loss data, the use of different or modified climate and climate index records and the use of additional data analysis techniques. Useful information would also be gained if data from additional tree-ring sites were included, particularly from sites at the lower treeline. A broader network of tree-ring data from a range of different sites would help disentangle the various factors affecting tree growth in this part of the world. After these issues are taken into consideration, a streamflow reconstruction for the Río Santa Cruz is certainly a feasible next-step toward understanding the natural hydroclimatic variability of southeastern Patagonia.

Acknowledgements

I am deeply grateful to Drs. Jan Esper and Martin Grosjean for allowing me the latitude to pursue my personal research interests through this project and to the University of Bern's Graduate School of Climate Science for funding my Master's thesis work. Many sincere thanks also to Drs. David Frank and Ricardo Villalba for their generous guidance and to my colleagues at the WSL for their support and enthusiasm. I am especially grateful to Drs. Valerie Trouet and Stephanie McAfee for their helpful revisions and professional support and to my parents for their unceasing love and encouragement through the ups, downs and long distances.

References

Literature:

Akkemik, U., et al. (2008), Tree-ring reconstructions of precipitation and streamflow for north-western Turkey, *Int. J. Climatol., 28*, 173-183.

Alexandersson, H. (1986), A homogeneity test applied to precipitation data, *Journal of Climatology, 6*, 661-675.

Aniya, M. (1999), Recent glacier variations of the Hielos Patagonicos, South America, and their contribution to sea-level change, *Arct. Antarct. Alp. Res., 31*, 165-173.

Aniya, M., et al. (1996), The use of satellite and airborne imagery to inventory outlet glaciers of the Southern Patagonia Icefield, South America, *Photogrammetric Engineering and Remote Sensing, 62*, 1361-1369.

Aniya, M., et al. (1997), Recent glacier variations in the Southern Patagonia Icefield, South America, *Arctic and Alpine Research, 29*, 1-12.

Aravena, J. C., et al. (2002), Tree-ring growth patterns and temperature reconstruction from *Nothofagus pumilio* (Fagaceae) forests at the upper tree line of southern Chilean Patagonia, *Revista Chilena De Historia Natural, 75*, 361-376.

Axelson, J. N., et al. (2009), New reconstructions of streamflow variability in the South Saskatchewan River Basin from a network of tree ring chronologies, Alberta, Canada, *Water Resour. Res., 45*.

Barnett, T. P., et al. (2005), Potential impacts of a warming climate on water availability in snow-dominated regions, *Nature, 438*, 303-309.

Bates, B. C., et al. (Eds.) (2008), *Climate Change and Water*, 210 pp., IPCC Secretariat, Geneva.

Blasing, T. J., and D. N. Duvick (1981), Dendroclimatic calibration and verification using regionally averaged and single station precipitation data, *Tree-Ring Bulletin, 41*, 37-43.

Boninsegna, J. A., et al. (1989), Dendrochronological studies in Tierra del Fuego, Argentina, *Quaternary of South America and Antarctic Peninsula, 7*, 305-326.

Bradley, R. S., and P. D. Jones (1992), *Climate Since A.D. 1500*, 679 pp., Routledge, London.

Briffa, K. R. (1995), Interpreting high resolution proxy climate data - The example of dendroclimatology, *Analysis Of Climate Variability - Applications Of Statistical Techniques*, 77-94.

Briffa, K. R., et al. (1990), A 1,400-year tree-ring record of summer temperatures in Fennoscandia, *Nature, 346*, 434-439.

Brito-Castillo, L., et al. (2003), Reconstruction of long-term winter streamflow in the Gulf of California continental watershed, *J. Hydrol., 278*, 39-50.

Büntgen, U., et al. (in press), Reduced climate sensitivity of Alpine tree growth at its Mediterranean margin, *Clim. Change*.

Carey, M. (2005), Living and dying with glaciers: people's historical vulnerability to avalanches and outburst floods in Peru, *Global and Planetary Change, 47*, 122-134.

Carson, E. C., and J. S. Munroe (2005), Tree-ring based streamflow reconstruction for Ashley Creek, northeastern Utah: implications for palaeohydrology of the southern Uinta Mountains, *The Holocene, 15*, 602-611.

Case, R. A., and G. M. MacDonald (2003), Tree ring reconstructions of streamflow for three Canadian Prairie rivers, *Journal Of The American Water Resources Association*, *39*, 703-716.

Chen, J. L., et al. (2007), Patagonia icefield melting observed by gravity recovery and climate experiment (GRACE), *Geophys. Res. Lett.*, *34*.

Christie, D. A., et al. (2009), El Niño-Southern Oscillation signal in the world's highest-elevation tree-ring chronologies from the Altiplano, Central Andes, *Palaeogeography, Palaeoclimatology, Palaeoecology*, *281*, 309-319.

Cleaveland, M. K. (2000), A 963-year reconstruction of summer (JJA) stream flow in the White River, Arkansas, USA, from tree-rings, *The Holocene*, *10*, 33-41.

Cobos, D. R., and J. A. Boninsegna (1983), Fluctuations of some glaciers in the upper Atuel River basin, Mendoza, Argentina, *Quaternary of South America and Antarctic Peninsula*, *1*, 61-82.

Cook, E. R. (1987), The decomposition of tree-ring series for environmental studies, *Tree-Ring Bulletin*, *47*, 37-59.

Cook, E.R., R.D. D'Arrigo, and K.J. Anchukaitis. 2008. ENSO reconstructions from long tree-ring chronologies: Unifying the differences? Talk presented at a special workshop on "Reconciling ENSO Chronologies for the Past 500 Years", held in Moorea, French Polynesia on April 2-3, 2008.

Cook, E. R., and R. L. Holmes (1986), Users manual for Program ARSTAN, in *Tree-ring chronologies of western North America: California, eastern Oregon and northern Great Basin*, edited by R. L. Holmes, et al., pp. 50-60, LTRR, University of Arizona, Tucson.

Cook, E. R., and G. C. Jacoby (1983), Potomac River Streamflow Since 1730 as Reconstructed by Tree Rings, *Journal of Applied Meteorology*, *22*, 1659-1672.

Cook, E. R., et al. (1999), Drought reconstructions for the continental United States, *Journal of Climate*, *12*, 1145-1162.

Cook, E. R., and K. Peters (1981), The smoothing spline: a new approach to standardizing forest interior tree-ring width series for dendroclimatic studies, *Tree-Ring Bulletin*, *41*, 45-53.

Cwielong, P. P., and M. Rajchenberg (1995), Wood-rotting fungi on *Nothofagus pumilio* in Patagonia, Argentina, *European Journal of Forest Pathology*, *25*, 47-60.

D'Arrigo, R., and G. Jacoby (1991), A 1000-year record of winter precipitation from northwestern New Mexico, USA: a reconstruction from tree-rings and its relation to El Niño and the Southern Oscillation., *The Holocene*, *1*, 95-101.

D'Arrigo, R., and R. Villalba (2000), Review of dendroclimatic research at high latitudes in South America: Indicators of atmosphere-ocean climate variability, in *Dendrochronology in Latin America*, edited by F. A. Roig, pp. 271-282, EDIUNC, Mendoza, Argentina.

Daniels, L. D., and T. T. Veblen (2000), ENSO effects on temperature and precipitation of the Patagonian-Andean region: implications for biogeography, *Phys. Geogr.*, *21*, 223-243.

Daniels, L. D., and T. T. Veblen (2004), Spatiotemporal influences of climate on altitudinal treeline in northern Patagonia, *Ecology*, *85*, 1284-1296.

Depetris, P. J., and A. I. Pasquini (2000), The hydrological signal of the Perito Moreno Glacier damming of Lake Argentino (southern Andean Patagonia): the connection to climate anomalies, *Global and Planetary Change*, *26*, 367.

DiFilippo, A., et al. (2007), Bioclimatology of beech (Fagus sylvatica L.) in the Eastern Alps: spatial and altitudinal climatic signals identified through a tree-ring network, *Journal of Biogeography*, *34*, 1873-1892.

DGA, Dirección General de Aguas. (1987), Balance Hídrico de Chile, edited by El Ministerio de Obras Públicas, p. 59, Santiago, Chile.

Donoso, C. (1993), *Bosques templados de Chile y Argentina: variación, estructura y dinámica*, 2 ed., 484 pp., Editorial Universitaria, Santiago de Chile.

Earle, C. J. (1993), Asynchronous droughts in California streamflow as reconstructed from tree rings, *Quaternary Research*, *39*, 290-299.

Esper, J., et al. (2003), Tests of the RCS method for preserving low-frequency variability in long tree-ring chronologies, *Tree-Ring Research*, *59*, 81-98.

Esper, J., et al. (2007), Long-term drought severity variations in Morocco, *Geophys. Res. Lett.*, *34*.

Francou, B., et al. (2003), Tropical climate change recorded by a glacier of the central Andes during the last decades of the 20th century: Chacaltaya, Bolivia, 16°S, *Journal of Geophysical Research*, *108*, 4154.

Fritts, H. C. (1971), Dendroclimatology and dendroecology, *Quaternary Research*, *1*.

Fritts, H. C. (1976), *Tree-Rings and Climate*, 567 pp., Academic Press, London.

Garreaud, R. D., et al. (2009), Present-day South American climate, *Palaeogeography, Palaeoclimatology, Palaeoecology*, *281*, 180-195.

Gea-Izquierdo, G., et al. (2009), Climate-growth variability of Quercus ilex L. west Iberian open woodlands of different stand density, *Annals of Forestry Science*, *66*, 802p801-802p812.

Gedalof, Z., et al. (2004), Columbia River flow and drought since 1750, *Journal Of The American Water Resources Association*, *40*, 1579-1592.

Gou, X. H., et al. (2007), Rapid tree growth with respect to the last 400 years in response to climate warming, northeastern Tibetan Plateau, *Int. J. Climatol.*, *27*, 1497-1503.

Graumlich, L. J., et al. (2003), Upper Yellowstone River flow and teleconnections with Pacific basin climate variability during the past three centuries, *Clim. Change*, *59*, 245-262.

Holmes, R. L. (1983), Computer-assisted quality control in tree-ring dating and measurement, *Tree Ring Bulletin*, *43*.

Holmes, R. L., et al. (1979), Extension Of River Flow Records In Argentina From Long Tree-Ring Chronologies, *Water Resour. Bull.*, *15*, 1081-1085.

Ibarzabal, T., et al. (1996), Recent climate changes in southern Patagonia, *Bulletin of Glacier Research*, *14*, 29-36.

Jobbágy, E. G., et al. (1995), Estimación de la precipitación y de su variabilidad interannual a partir de información geográfica en el NW de Patagonia, Argentina, *Ecología Austral*, *5*, 47-53.

Jones, P. D., et al. (1984), Riverflow reconstruction from tree rings in southern Britain, *Int. J. Climatol.*, *4*, 461-472.

Jones, P. D., et al. (1986), Southern Hemisphere surface air temperature variations: 1851-1984, *Journal of Climate and Applied Meteorology*, *25*, 1214-1230.

Kahya, E., and S. Kalayci (2004), Trend analysis of streamflow in Turkey, *J. Hydrol.*, *289*, 128-144.

Kaser, G., and C. Georges (1990), Glacier flucuations and climate in the Cordillera Blanca, Peru, *Annals of Glaciology*, *14*, 136-140.

Kaser, G. v., et al. (2001), Gletscher in den Hochgebirgen der niederen Breiten, *Innsbrucker Jahresbericht 2001/02*, 82-103.

Kendall, M. G. (1975), *Rank Correlation Methods*, Charles Griffin, London.

Lara, A., et al. (2001), Dendroclimatology of high-elevation Nothofagus pumilio forests at their northern distribution limit in the central Andes of Chile, *Can. J. For. Res.-Rev. Can. Rech. For.*, *31*, 925-936.

Lara, A., et al. (2005a), The potential use of tree-rings to reconstruct streamflow and estuarine salinity in the Valdivian Rainforest eco-region, Chile, *Dendrochronologia*, *22*, 155.

Lara, A., et al. (2008), A 400-year tree-ring record of the Puelo River summer-fall streamflow in the Valdivian Rainforest eco-region, Chile, *Clim. Change*, *86*, 331-356.

Lara, A., et al. (2005b), Spatial and temporal variation in Nothofagus pumilio growth at tree line along its latitudinal range (35 degrees 40-55 degrees S) in the Chilean Andes, *Journal Of Biogeography*, *32*, 879-893.

Lough, J. M., and H. C. Fritts (1985), The Southern Oscillation and tree rings: 1600-1961, *Journal of Climate and Applied Meteorology*, *24*, 952-966.

Mann, H. B. (1945), Nonparametric tests against trend, *Econometrica*, *13*, 245-259.

Mark, B. G., and G. O. Seltzer (2003), Tropical glacier meltwater contribution to streamflow: a case study in the Cordillera Blanca, Peru, *Journal of Glaciology*, *49*, 271-281.

Masiokas, M., and R. Villalba (2004), Climatic significance of intra-annual bands in the wood of *Nothofagus pumilio* in southern Patagonia, *Trees- Structure and Function*, *18*, 696-704.

Masiokas, M., et al. (2008), 20th-century glacier recession and regional hydroclimatic changes in northwestern Patagonia, *Global and Planetary Change*, *60*, 85-100.

McClurg, S. (2007), 1922-2007: 85 Years of the Colorado River Compact, in *Western Water*, edited, Water Education Foundation.

Meko, D., and D. A. Graybill (1995), Tree-ring reconstruction of Upper Gila River discharge, *Water Resour. Bull.*, *31*, 605-616.

Meko, D., et al. (2001), Sacremento River flow reconstructed to A.D. 869 from tree rings, *Journal Of The American Water Resources Association*, *37*, 1029-1039.

Meko, D. M., and C. A. Woodhouse (2005), Tree-ring footprint of joint hydrologic drought in Sacramento and Upper Colorado river basins, western USA, *J. Hydrol.*, *308*, 196-213.

Naruse, R., et al. (1997), Thinning and retreat of Glaciar Upsala, and an estimate of annual ablation changes in southern Patagonia, *Annals of Glaciology*, *24*, 38-42.

Norton, D. A. (1983), Modern New Zealand tree-ring chronologies, *Tree-Ring Bulletin*, *43*, 39-49.

Norton, D. A. (1987), Reconstruction of past river flow and precipitation in Canterbury, New Zealand from analysis of tree-rings, *Journal of Hydrology (N.Z.)*, *26*, 161-174.

OECD (2008), *OECD Environmental Outlook to 2030*, 520 pp., Organisation for Economic Co-operation and Development, Paris.

Paruelo, J. M., et al. (1998), The climate of Patagonia: general patterns and controls on biotic processes, *Ecología Austral*, *8*, 85-101.

Pasquini, A. I., et al. (2008), Climate change and recent water level variability in Patagonian proglacial lakes, Argentina, *Global and Planetary Change*, *63*, 290.

Pederson, N., et al. (2001), Hydrometeorological Reconstructions for Northeastern Mongolia Derived from Tree Rings: 1651–1995, *Journal Of Climate*, *14*, 872-881.

Peña, H., and R. Gutiérrez (1992), Statistical analysis of precipitation and air temperature in the Southern Patagonia Icefield, in *Glaciological Researches in Patagonia 1990*, edited by R. Naruse and M. Aniya, pp. 95-107, Japanese Society of Snow and Ice.

Peterson, T. C., and R. S. Vose (1997), An Overview of the Global Historical Climatology Network Temperature Database, *Bulletin of the American Meteorological Society*, *78*, 2837-2849.

Prohaska, F. (1976), The Climate of Argentina, Paraguay and Uruguay, in *Climates of Central and South America. World Survey of Climatology*, edited by W. Schwerdtfeger, pp. 13-112, Elsevier, Amsterdam, The Netherlands.

Quintela, R. M., et al. (1996), The probable impact of global change on the water resources of Patagonia, Argentina., in *Regional hydrological responses to climate change*, edited by J. A. A. Jones, pp. 389-407, Kluwer Academic Publishers, The Netherlands.

Quiroga, A. (2008), Construirán dos nuevas represas en Santa Cruz, in *Clarín*, edited, Buenos Aires.

Rasmussen, L. A., et al. (2007), Influence of upper air conditions on the Patagonia icefields, *Global and Planetary Change*, *59*, 203.

Rignot, E., et al. (2003), Contribution of the Patagonia Icefields of South America to sea level rise, *Science*, *302*, 434-437.

Rivera, A. (2004), Mass balance investigations at Glaciar Chico, Southern Patagonia Icefield, Chile, in *PhD thesis*, edited, p. 303, University of Bristol, UK.

Rivera, A., et al. (2002), Use of remote sensing and field data to estimate the contribution of Chilean glaciers to the sea level rise, *Annals of Glaciology*, *34*, 367-372.

Rivera, A., et al. (2005), Glacier shrinkage and negative mass balance in the Chilean Lake District (40°S), *Hydrological Sciences Journal*, *50*, 963-974.

Rivera, A., et al. (2000), Variaciones recientes de glaciares en Chile, *Revista de Investigaciones Geográficas*, *34*.

Roig, F. A., and R. Villalba (2008), Understanding Climate from Patagonian Tree Rings, in *Developments in Quaternary Science*, edited, p. 411, Elsevier.

Rösenbluth, B., et al. (1995), Recent climatic changes in western Patagonia, *Bulletin of Glacier Research*, *13*, 127-132.

Rösenbluth, B., et al. (1997), Recent temperature variations in southern South America, *Int. J. Climatol.*, *17*, 67-85.

Schneider, C., et al. (2003), Weather observations across the southern Andes at 53S, *Phys. Geogr.*, *24*, 97-119.

Schulman, E. (1956), *Dendroclimatic changes in semiarid America*, University of Arizona Press, Tucson.

Schweingruber, F. H. (1988), *Tree rings: Basics and applications of dendrochronology*, 1 ed., 272 pp., D. Reidel Publishing Company, Dordrecht, The Netherlands.

Smith, L. P., and C. W. Stockton (1981), Reconstructed Stream Flow for the Salt and Verde Rivers From Tree-Ring Data, *Journal of the American Water Resources Association*, *17*, 939-947.

Srur, A. M., et al. (2008), Influences of climatic and CO2 concentration changes on radial growth of Nothofagus pumilio in Patagonia, *Revista Chilena De Historia Natural*, *81*, 239-256.

Stahle, D. W., and M. K. Cleaveland (1993), Southern Oscillation extremes reconstructed from tree rings of the Sierra Madre Occidental and southern Great Plains., *Journal Of Climate*, *6*, 129-140.

Stockton, C. W., and G. C. Jacoby (1976), Long-term surface water supply and streamflow trends in the Upper Colorado River Basin, *Lake Powell Research Project Bulletin*, *18*.

Thompson, D. W. J., and S. Solomon (2002), Interpretation of Recent Southern Hemisphere Climate Change, *Science*, *296*, 895-899.

Tikalsky, B. (2007), An 828-year streamflow reconstruction for the Jordan River drainage basin of northern Utah, 81 pp, Brigham Young University.

Timilsena, J., et al. (2007), Five hundred years of hydrological drought in the Upper Colorado River basin, *Journal Of The American Water Resources Association*, *43*, 798-812.

Trenberth, K. E. (1997), The definition of El Niño, *Bulletin of the American Meteorological Society*, *78*, 2771-2777.

Valladares, A. (2004), Cuenca del Río Santa Cruz, edited by Subsecretaría de Recursos Hídricos de Argentina, Secretaría de Obras Públicas.

Veblen, T. T., et al. (1996), Ecology of Southern Chilean and Argentinean *Nothofagus* forests, in *The Ecology and Biogeography of Nothofagus forests*, edited by T. T. Veblen, et al., p. 403, Yale University Press, New Haven and London.

Villalba, R. (2007), Tree-ring evidence for tropical-extratropical influences on climate variability along the Andes in South America, *PAGES News*, *15*.

Villalba, R., et al. (1997a), Recent trends in tree-ring records from high elevation sites in the Andes of northern Patagonia, *Clim. Change*, *36*, 425-454.

Villalba, R., et al. (1997b), Sea-level pressure variability around Antarctica since A.D. 1750 inferred from subantarctic tree-ring records., *Climate Dynamics*, *13*, 375-390.

Villalba, R., et al. (1998), Tree-ring based reconstructions of northern Patagonia precipitation since A.D. 1600, *The Holocene*, *8*, 659-674.

Villalba, R., et al. (2003), Large-scale temperature changes across the southern Andes: 20th-century variations in the context of the past 400 years, *Clim. Change*, *59*, 177-232.

Villalba, R., et al. (1990), Climate, Tree-Ring, and Glacial Fluctuations in the Rio Frias Valley, Rio Negro, Argentina, *Arctic and Alpine Research*, *22*, 215.

Villalba, R., and T. T. Veblen (1997), Regional patterns of tree population age structures in northern Patagonia: Climatic and disturbance influences, *Journal of Ecology*, *85*, 113-124.

Villalba, R., and T. T. Veblen (1998), Influences of large-scale climatic variability on tree mortality in northern Patagonia, *Ecology*, *79*, 2624-2640.

Warren, C. R., and D. E. Sugden (1993), The Patagonian Icefields - A Glaciological Review, *Arctic and Alpine Research*, *25*, 316-331.

Watson, T. A., et al. (2009), Reconstructed Streamflows For The Headwaters Of The Wind River, Wyoming, United States, *Journal Of The American Water Resources Association*, *45*, 224-236.

Waylen, P., et al. (2000), Interannual and interdecadal variability in stream flow from the Argentine Andes, *Phys. Geogr.*, *21*, 452-465.

Wigley, T. M. L., et al. (1986), On the average value of correlated time series, with applications in dendrochronology and hydrometeorology, *Journal of Applied Meteorology*, *23*, 201-213.

Wilks, D. (2006), *Statistical Methods in the Atmospheric Sciences*, 2nd ed., 627 pp., Elsevier, Boston.

Woodhouse, C. A., et al. (2006), Updated streamflow reconstructions for the Upper Colorado River Basin, *Water Resour. Res.*, *42*.

Yuan, Y., et al. (2007), The potential to reconstruct Manasi River streamflow in the northern Tien Shan Mountains (NW China), *Tree-Ring Research*, *63*, 81-93.

Yue, S., et al. (2002), Power of the Mann-Kendall and Spearman's rho tests for detecting monotonic trends in hydrological series, *J. Hydrol.*, *259*, 254-271.

Online sources:

CPC, Climate Prediction Center. Web: http://www.cpc.ncep.noaa.gov/data/indices/ [08/24/2009]

CRU, University of East Anglia Climate Research Unit. CRU Datasets. British Atmospheric Data Centre, 2008. Web: http://badc.nerc.ac.uk/data/cru. [03/15/2009]

GHCN, Global Historical Climatology Network, National Climatic Data Center. Web: http://www.ncdc.noaa.gov/oa/climate/ghcn-monthly/index.php [03/18/2009]

GISS, Goddard Institute for Space Sciences. Web: http://data.giss.nasa.gov/gistemp/station_data/ [03/15/2009]

KNMI, The Royal Netherlands Meteorological Institute. "Climate Explorer- Monthly Station Data." Web: http://climexp.knmi.nl/. [03/21/2009]

NCAR, National Center for Atmospheric Research. "An informed guide to climate data sets." 10 Jan 2003. http://www.cgd.ucar.edu/cas/guide/Data/hulme_p.html. [10/11/2009]

Rinntech. Web: http://www.rinntech.com [01/20/2009]

Subsecretaría de Recursos Hídricos de Argentina (2004), Estadística Hidrológica - República Argentina, http://www.hidricosargentina.gov.ar/estad2004/act-xcuencas.htm. [09/20/2008]

Appendix I

International Tree-Ring Data Bank species codes

ABLA	Abies lasiocarpa
ABBN	Abies bornmuelleriana
ABCO	Abies concolor
ARAR	Araucaria araucana
AUCH	Austrocedrus chilensis
JUOC	Juniperus occidentalis
JUPR	Juniperus przewalski
LALY	Lariz llyali
LASI	Larix sibirica
NOSO	Nothofagus solandri
PCMA	Picea mariana
PCSH	Picea schrenkiana
PIBA	Pinus balfouriana
PICO	Pinus contorta
PIED	Pinus edulis
PIFL	Pinus flexilis
PIJE	Pinus jeffreyi
PILA	Pinus lambertiana
PILO	Pinus longaeva
PIMO	Pinus monophylla
PINI	Pinus nigra
PIPO	Pinus ponderosa
PIRI	Pinus roxburghii
PISF	Pinus strobiformis
PISY	Pinus sylvestris
PLUV	Pilgerodendron uviferum
PSME	Psuedotsuga menzeisii
QUAL	Quercus alba
QULO	Quercus lobata
QUPE	Quercus petraea
QUPR	Quercus prinus
QURO	Quercus robur
SEGI	Sequoiadendron giganteum
TADI	Taxodium distichum
TSCA	Tsuga canadensis
TSME	Tsuga mertensiana

Appendix II

List of figures

Appendix III

List of tables